Drug Design, Development and Therapy

Dovepress
Taylor & Francis Group

Open Access Full Text Article

ORIGINAL RESEARCH

Kuoxin Decoction Alleviated Left Ventricular Remodeling by Inhibiting Cardiomyocyte Apoptosis Through ASK1/JNK/Cx43 Signaling Pathway in cTnTR141W Transgenic Mice and in vitro

Mengjiao Ma[1,*], Hua Fan[1,*], Yidan Dong[1,2], Tianyi Feng[1], Longping Peng[1], Maolin Zhou[1], Feifei Liu[1], RueyJyh Lee[1], Rongxue Wu[3], Qiong Wu[1,3], Youhua Wang[1]

[1]Department of Cardiology, Longhua Hospital, Shanghai University of Traditional Chinese Medicine, Shanghai, People's Republic of China; [2]Department of Cardiology, Yueyang Hospital of Integrated Traditional Chinese and Western Medicine, Shanghai University of Traditional Chinese Medicine, Shanghai, People's Republic of China; [3]Department of Medicine/Cardiology, Biological Sciences Division, University of Chicago, Chicago, IL, USA

*These authors contributed equally to this work

Correspondence: Youhua Wang; Qiong Wu, Department of Cardiology, Longhua Hospital, Shanghai University of Traditional Chinese Medicine, Shanghai, People's Republic of China, Email doctorwyh@163.com; wuqiong1203@126.com

Purpose: Combined with RNA sequencing and experimental verification methods to investigate KXD's potential role and underlying mechanisms in cTnT^{R141W} transgenic mice and H9c2 cells.

Methods: UPLC-Q-TOF-MS analysis was employed to identify the absorbed constituents from KXD in mice blood. cTnT^{R141W} transgenic mice were given with KXD via gavage for 4 weeks. Cardiac remodeling was evaluated by echocardiography, heart weight index, H&E staining, Masson staining, and WGA staining. The potential therapeutic target of KXD was identified through RNA sequencing. H9c2 cells were stimulated with DOX and KXD in vitro. Tunel staining, Immunofluorescence, Transmission electron microscopy, qRT-PCR, and Western blot were used to evaluate cardiomyocyte apoptosis and gap junction remodeling.

Results: 11 compounds from KXD were identified in the blood. KXD improved cardiac dysfunction and alleviated interstitial fibrosis and cardiomyocyte hypertrophy in cTnT^{R141W} transgenic mice. The mechanistic investigations of RNA sequencing revealed that regulating apoptosis and gap junctions may be potential processes for KXD. KXD inhibited cardiomyocyte apoptosis, and promoted the expression of Connexin 43, a key protein of gap junctions, while also inhibiting the phosphorylation of ASK1 and JNK in cTnT^{R141W} transgenic mice and H9c2 cells.

Conclusion: KXD attenuated left ventricular remodeling and cardiomyocyte apoptosis in cTnT^{R141W} transgenic mice and H9c2 cells, potentially through modulation of the ASK1/JNK/Cx43 signaling pathway. These findings provide valuable insights into the therapeutic potential of KXD in mitigating DCM.

Keywords: Kuoxin Decoction, cardiomyocyte apoptosis, gap junctions, ASK1/JNK signaling pathway, dilated cardiomyopathy

Introduction

Dilated cardiomyopathy (DCM) is a primary and heterogeneous cardiomyopathy characterized by left ventricular (LV) enlargement, myocardial systolic dysfunction, and progressive ventricular remodeling.[1,2] It is associated with a high risk of sudden death, poor prognosis, and severe complications, including intractable heart failure, malignant arrhythmias, thromboembolism, and cardiogenic shock. In China, the case fatality rate of DCM is alarmingly high at 42.24% after 52 months of follow-up, highlighting its role as a major cause of sudden death.[3] Globally, DCM is also one of the leading causes of heart transplantation in both children and adults.[3] Despite its prevalence and severity, the disease continues to pose a significant challenge due to its unknown etiology, complex pathogenesis, and the absence of effective targeted therapies.[1,3,4]

Received: 10 February 2025
Accepted: 23 July 2025
Published: 4 August 2025

Graphical Abstract

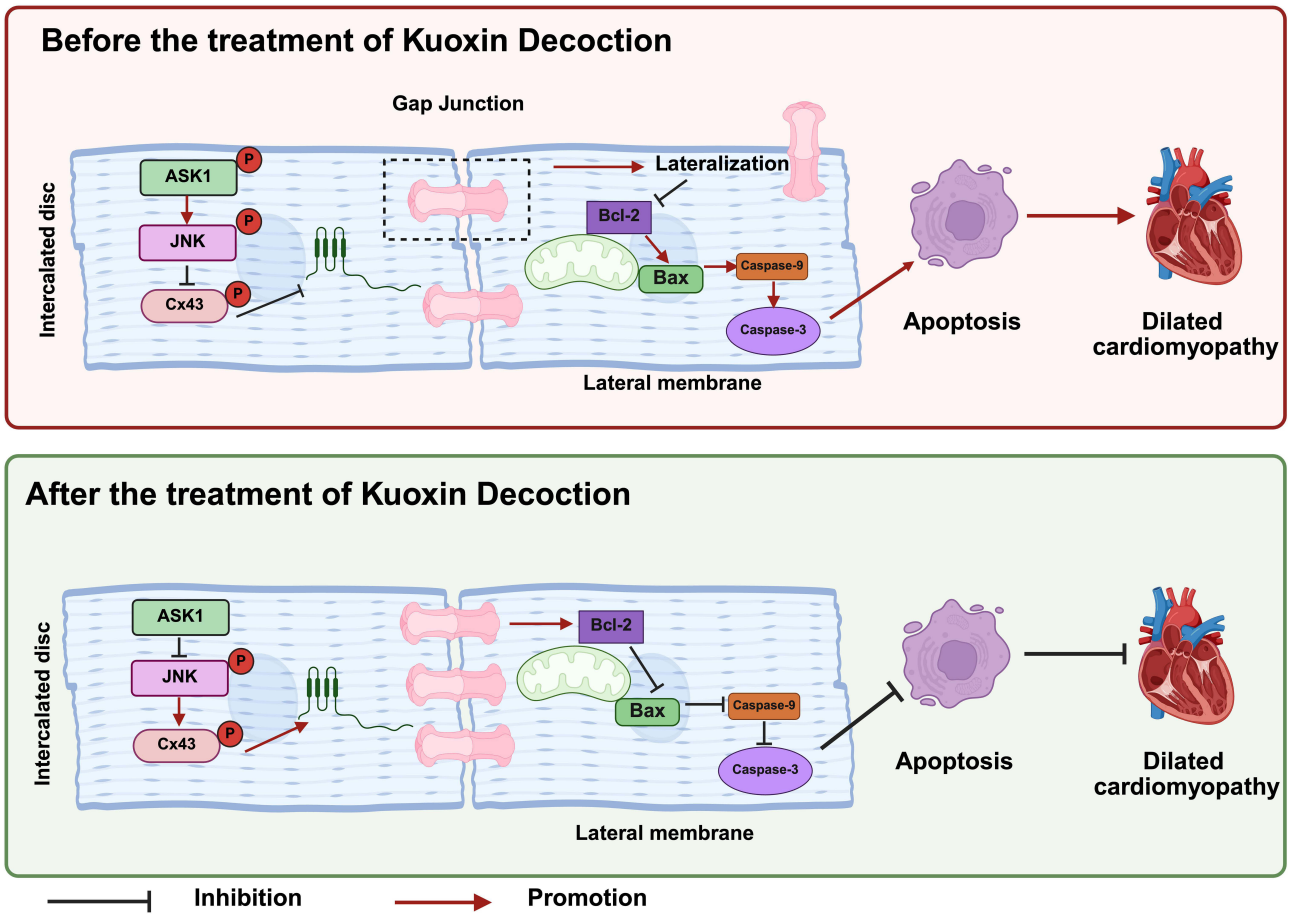

Approximately 20~35% of DCM patients have a family history, with the most common familial form being autosomal dominant.[1] The R141W missense mutation in the tropomyosin-binding region of cardiac troponin T (cTnT) has been identified as a major cause of familial dilated cardiomyopathy (FDCM).[5] Transgenic mice expressing $cTnT^{R141W}$, generated by inserting the mutant gene downstream of the α-MHC promoter, develop cardiac dysfunction with dilated chambers, thin walls, and impaired cardiac function, mirroring DCM pathology.[6–8] Doxorubicin (DOX), an anthracycline antibiotic, is used to treat various types of cancer.[9,10] Unfortunately, high doses of DOX put cancer patients at risk of developing DCM.[2,11] DOX-induced cardiotoxicity leads to cardiomyocyte injury by triggering apoptosis, ferroptosis, necroptosis, and other cell death pathways.[12] To explore the mechanisms of DCM and potential therapies, our study uses two models: $cTnT^{R141W}$ transgenic mice for genetic DCM and DOX-treated H9c2 cardiomyocytes for chemotherapy-induced injury, providing a comprehensive platform for understanding DCM progression and identifying new interventions.

Cardiac remodeling is the fundamental pathological process underlying DCM. In DCM mouse models, there is a significant increase in cardiomyocyte apoptosis within the heart tissue.[13] The apoptosis results in a reduction of cardiomyocytes, cell hypertrophy, interstitial fibrosis, and alterations in cardiac chamber structure, ultimately triggering left ventricular remodeling. Given that cardiomyocytes are terminally differentiated cells without regenerative capacity, the loss of cardiomyocytes due to apoptosis plays a critical role in the progression of left ventricular remodeling and dysfunction in DCM.[14]

Connexin 43 (Cx43) is a crucial protein of gap junctions (GJs), and its remodeling involves increased internalization, lateralization, and degradation.[15] It has been confirmed that there are Cx43 remodeling and gap junction abnormalities in

various cardiomyopathy and myocardial ischemia models.[15,16] Gap junction remodeling is closely related to apoptosis, as numerous studies have shown that the degradation of Cx43 phosphorylation not only activates the mitochondrial apoptotic pathway but also triggers exogenous apoptosis by activating death receptors.[17,18] Therefore, alleviating cardiomyocyte apoptosis by improving gap junction remodeling is a potential therapy for DCM. The ASK1/JNK pathway is closely associated with apoptosis and gap junction remodeling, with Cx43-mediated intercellular communication exacerbating oxidative stress signaling and inducing excessive apoptosis via the ASK1-JNK/p38 signaling pathway.[19] Additionally, our previous studies using protein chip technology revealed a significant increase in ASK1 and JNK levels in the hearts of DCM rats induced by DOX.

Current pharmacological treatments for DCM primarily focus on managing heart failure. However, traditional anti-heart failure drugs are often limited by their propensity to cause hypotension or their modest impact on symptom improvement. Given these challenges, traditional Chinese medicine (TCM) offers a promising complementary approach by targeting the underlying pathophysiological processes while enhancing cardiac function.[20] TCM not only supports myocardial recovery but also mitigates the side effects of conventional therapies, providing a more holistic strategy for DCM management. Integrating TCM with standard treatments may optimize therapeutic outcomes and improve patients' quality of life. Kuoxin Decoction (KXD), developed by Professor Duan Zhou, a renowned Chinese medicine specialist, has been used clinically for over two decades to treat DCM. These ingredients work synergistically to tonify Qi, nourish Yin, warm Yang, activate blood circulation, transform phlegm, and promote fluid metabolism. Kuoxin Decoction (KXD), a TCM formula, has been used to treat DCM, with clinical studies have shown that combining KXD with Western medicine significantly improved cardiac function, alleviated clinical symptoms, and reduced the readmission rate for heart failure compared to Western medicine alone.[21,22] Animal studies further demonstrated that KXD improved left ventricular remodeling in DCM models.[23–25] However, whether KXD can alleviate DCM by regulating gap junctions and apoptosis remains unclear. Therefore, this study aims to explore the potential of KXD in mitigating gap junction remodeling and apoptosis in DCM and to elucidate the complex molecular mechanisms underlying its therapeutic effects.

Materials and Methods

Preparation of Kuoxin Decoction Lyophilized Powder

As detailed in Table 1, KXD consists of *Astragalus mongholicus* Bunge (Huangqi), *Polygonatum kingianum* Collett & Hemsl (Huangjing), *Salvia miltiorrhiza* Bunge (Danshen), *Neolitsea cassia* (L) Kosterm (Guizhi), *Trichosanthes kirilowii* Maxim (Gualoupi), *Vitex negundo* L (Huangjingzi), *Ganoderma lucidum* (Leyss. Ex Fr). Karst (Lingzhi), *Whitmania pigra* Whitman

Table 1 Components of Kuoxin Decoction (KXD)

No.	Chinese Name/*Pinyin*	Scientific Name	Dosage Used	Part and Form Used	Place of Origin (China)
1	Sheng Huang Qi	*Astragalus mongholicus* Bunge	30g	Dried root	Neimenggu
2	Huang Jing	*Polygonatum kingianum* Collett & Hemsl	30g	Dried rhizome	Yunnan
3	Ling Zhi	*Ganoderma lucidum* (Leyss. Ex Fr.) Karst	9g	Dried fruiting body	Guizhou
4	Dan Shen	*Salvia miltiorrhiza* Bunge	15g	Dried root and rhizome	Hebei
5	Shui Zhi	*Whitmania pigra* Whitman	6g	Dried whole body	Jiangsu
6	Gua Lou Pi	*Trichosanthes kirilowii* Maxim	30g	Dried and ripe peel	Shandong
7	Gui Zhi	*Neolitsea cassia* (L.) Kosterm	3g	Dried twig	Guangdong
8	Huang Jing Zi	*Vitex negundo* L	9g	Dried and ripe fruit	Jiangsu
9	Mao Dong Qing	*Ilex pubescens* Hook. and Arn	30g	Dried root	Zhejiang
10	Mao Ren Shen	*Actinidia valvata* Dunn	30g	Dried root	Anhui

(Shuizhi), *Ilex pubescens* Hook. and Arn (Maodongqing), and *Actinidia valvata* Dunn (Maorenshen). The plant names could refer to Plants of the World Online (http://mpns.kew.org/mpns-portal/?_ga=1.111763972.1427522246.1459077346) and Pharmacopoeia of the People's Republic of China 2020 Edition (https://ydz.chp.org.cn/). Herbs of KXD were purchased from Shanghai Wanshicheng Pharmaceutical Co., Ltd. (Shanghai, China). All herbs were identified by Professor Lihong Wu, and the voucher specimens of the herbal pieces are deposited in the Herbarium of Institute of Chinese Materia Medica, Shanghai University of Traditional Chinese Medicine. The herbs were soaked and boiled in 30 L of water for 1 hour, and the mixture was filtered using a 325-mesh sieve. Reflux was extracted thrice, and the filtrates from thrice decoction steps were combined. After ethanol precipitation and lyophilization, Kuoxin Decoction lyophilized powder was prepared. The herbs of KXD (192g) were prepared into KXD lyophilized powder (14g), and the lyophilized powder was then preserved at −20°C for the following use. To ensure quality control, the active components in KXD have been verified by HPLC in our previous research.[26]

UPLC-Q-TOF-MS Analysis

The chemical constituents in KXD were analyzed using UPLC-Q-TOF-MS. The ACQUITY UPLC H-Class system (Waters, China) and AB Sciex Triple TOF® 4600 quadrupole-time of flight mass spectrometer (SCIEX, Germany) were used for mass spectrometry detection. Chromatographic separation was achieved on the Waters ACQUITY UPLC HSS T3 column (2.1×100 mm, 1.8 μm). The mobile phase ratio and flow rates were acetonitrile (A) and 0.1% aqueous formic acid (B). The gradient conditions were as follows: 0–3 min, 100% B; 3–7 min, 0–6% A and 100–94% B; 7–10 min, 6–10% A and 94–90% B; 10–25 min, 10–22% A and 90–78% B; 25–30 min, 22–40% A and 78–60% B; 30–38 min, 40–45% A and 60–55% B; 38–41 min, 45–95% A and 55–5% B; 41–44 min, 95% A and 5% B; 44–44.1 min, 95–0% A and 5–100% B; 44.1–47 min, 100% B. The column oven temperature was set at 30 °C, the flow rate was 0.3 mL/min, and the injection volumes for all samples were 5 μL. The mass spectrometry detection mode was ESI-negative/positive ion mode. Mass parameters were as follows: TOF mass range: 50–1700; ion source gas 1 and 2: 50 psi; curtain gas: 35 psi; ion spray voltage floating: −4500/5000 V.

To identify the absorbed constituents from KXD in mice serum, 12 mice were orally administered with KXD (9.1g/kg/d, five times the clinical equivalent dose[27]) for three consecutive days. Afterward, blank plasma and plasma after gavage (0.5 h, 1 h, and 2 h) were collected, respectively. UPLC-Q-TOF-MS was used to analyze the ingredients of KXD in the plasma.

Materials and Reagents

Masson's Trichrome Stain Kit (G1340) was purchased from Solarbio Life Sciences. Wheat Germ Agglutinin (WGA) (FL-1021-10) was purchased from Vectorlabs. Anti-Connexin 43 antibody (3512), anti-rabbit IgG (H+L) (4412S), anti-SAPK/JNK antibody (9252), anti-mouse IgG HRP-linked antibody (7076S), and anti-Rabbit IgG HRP-linked antibody (7074S) were obtained from Cell Signaling TECHNOLOGY. Beyotime Biotechnology provided One Step TUNEL Apoptosis Assay Kit (C1090). Anti-ASK1 antibody (131506) and anti-Fas antibody (ab82419) were purchased from Abcam. Anti-ASK1 phospho (Ser966) antibody (ARG51675), anti-SAPK/JNK phospho (Thr183 (221)/Tyr185 (223)) antibody (ARG51807), anti-Bcl-2 antibody (ARG55188), and anti-Bax antibody (ARG66247) were purchased from Arigo. Anti-GAPDH antibody (G9545) was purchased from Sigma. Captopril (Cap) was purchased from Changzhou pharmaceutical factory. DMEM (AH30006378) and fetal bovine serum (FBS) (10,270–106) were purchased from HyClone. Penicillin-streptomycin (15140–122) and trypsin-EDTA (0.25%) phenol red (25200–056) were obtained from Gibco. Doxorubicin (HY-15142) was purchased from MedChemExpress.

Animals

The $cTnT^{R141W}$ transgenic mice were generated by the Institute of Laboratory Animal Science, Chinese Academy of Medical Sciences, and exhibited DCM phenotypic characteristics consistent with those reported previously.[6,14] As shown in Figure 1, a full-length human cTnT cDNA was successfully cloned from human heart tissue through RT-PCR. Subsequently, its accuracy was verified by sequencing analysis. The T→C substitution at nucleotide position 520, which leads to the R141W mutation in the corresponding protein, was deliberately induced via oligonucleotide-mediated site-directed mutagenesis. The cTnT cDNA with the R141W mutation was inserted downstream of the α-MHC promoter. The entire transgenic expression cassette, composed of the α-MHC promoter and the human cTnT-Trp141 cDNA, was precisely excised from the transgenic

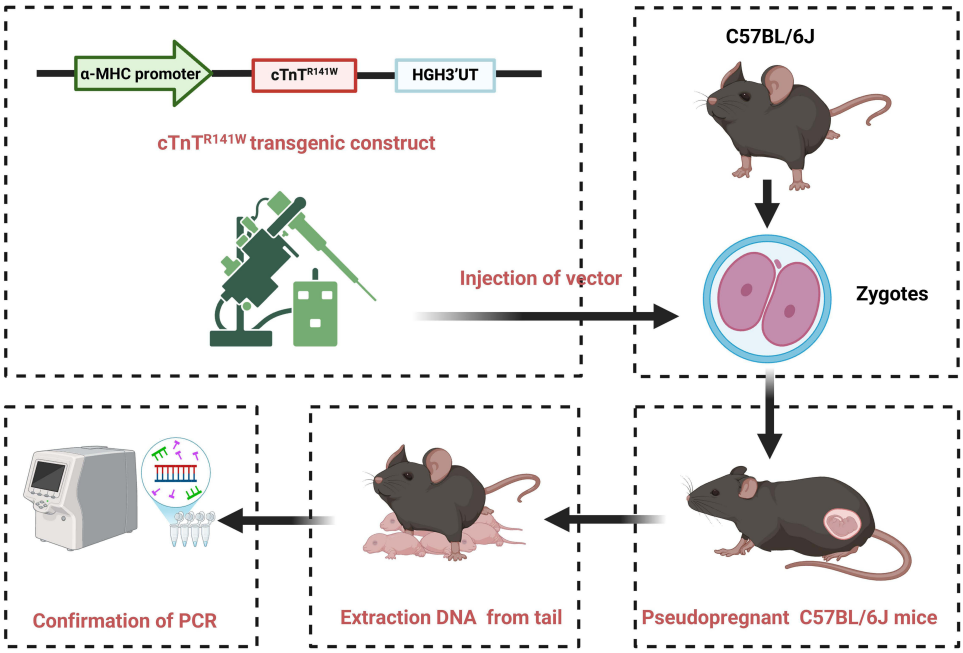

Figure 1 Construction process for cTnT^{R141W} transgenic mice. This presentation was created in BioRender. Ma, M. (2025) BioRender.com/69jqfx8.

plasmid using the restriction enzyme Sall. The fragment was purified, dissolved in Tris–HCl–EDTA, and injected into the pronucleus of zygotes harvested from C57BL/6J mice, and then the cTnT^{R141W} transgenic mice were generated. For the genotyping of transgenic mice, PCR was employed with the primers, 5′GAACAGGAGGAAGGCTGAGGATGAG and 5′ TATTTCCAGCGCCCGGTG ACTTTAG. All mice used in this study maintain the C57BL/6J genetic background.

A total of 44 mice were used in the study, consisting of 33 cTnT^{R141W} transgenic mice and 11 wide-type (WT) mice. Mice were raised at the Animal Experiment Center, Shanghai University of Traditional Chinese Medicine (SHUTCM). All animal procedures in this study strictly followed the Guidelines on Humane Treatment of Laboratory Animals (Ministry of Science and Technology of China, 2006). Animal experiments were approved by the Animal Care Committee of SHUTCM (Ethics protocol number: PZSHUTCM2302050003). The sample size was determined using the resource equation method, which indicated that 4–6 mice per group would be sufficient. Considering the multiple experimental measurements in our study, we allocated 11 mice to each group to ensure robust statistical power. The 3.5-month-old cTnT^{R141W} transgenic mice were randomly divided into three groups: the cTnT^{R141W} group (n=11), the KXD group (n=11), and the captopril group (n=11). Age-matched non-transgenic littermates were used as WT controls (n=11). The dosage of KXD used in cTnT^{R141W} transgenic mice was converted from the clinical dosage based on body surface area. In the KXD group, transgenic mice were given KXD (1.82g/kg/d) via gavage for 4 weeks. Transgenic mice were given captopril (3.25mg/kg/d) via gavage in the Cap group for 4 weeks. In the WT group and the cTnT^{R141W} group, mice were given 0.9% NaCl for 4 weeks.

Echocardiography

After anesthesia with isoflurane, echocardiography was measured in anesthetized mice using supine position. Left ventricular end-diastolic dimension (LVEDD), left ventricular end-systolic dimension (LVESD), left ventricular end-diastolic diameter (LVDd), left ventricular end-systolic diameter (LVDs), left ventricular posterior wall (LVPW), left ventricular anterior wall (LVAW), the ejection fraction (EF), and fractional shortening (FS) were obtained by M-mode.

Heart Weight Index

After the mice's body weight (BW) was recorded, the mice were anesthetized and the eyeball blood was collected. The heart weight (HW), the lung weight (LW), and the tibial length (TL) of the left leg were recorded, and the ratio of HW/BW, HW/LW, and HW/TL was calculated.

https://doi.org/10.2147/DDDT.S517404

Histology

Part of the cardiac tissue was fixed in 4% paraformaldehyde for 48 hours and embedded after dehydration. The rest was embedded in the O.C.T. Compound and frozen in liquid nitrogen. After cardiac tissue was dewaxed, Hematoxylin and eosin (H&E) staining, Masson staining, and wheat germ agglutinin staining were used to observe histopathological changes.

Immunofluorescent

Cardiac tissues were embedded in O.C.T. Compound and cut at a thickness of 7μm. After O.C.T. Compound was washed with PBS, heart tissue sections were blocked by 5% BSA for 1 hour, and incubated with Cx43 antibody overnight at 4°C. After washing with PBS, the anti-Rabbit IgG HRP-linked antibody and anti-WGA antibody were added and incubated for 1 hour. Afterward, the tunel detection solution was added. Images were taken to evaluate the location and expression of Cx43 and apoptosis in heart tissue.

Transmission Electron Microscopy (TEM)

Processing and TEM were conducted as previously described.[28] Gap junctions are observed at the intercalated disk between two neighboring cardiomyocytes at a magnification of ×8200 using a transmission electron microscope. Then, the integrity of the gap junction was evaluated and the width of the gaps was randomly measured at ten points with ImageJ software.[29]

RNA-Sequencing (RNA-Seq)

Total RNA was extracted from hearts, and Oligo(dT)-attached magnetic beads were used to purify mRNA. Purified mRNA was broken into fragments about 300bp, and then first-strand cDNA was reversed transcription from purified mRNA fragments, followed by a second-strand cDNA synthesis. End Repair Mix and RNA Index Adapters were added for purification and fragment sorting, and PCR amplification was used for sorted products and the final library was obtained. Finally, RNA-seq was performed on the NovaSeq X Plus platform. Based on the quantitative results of expression levels, differentially expressed genes (DEGs) between two groups were obtained using DESeq2 with a threshold of fold change ≥2 and P value <0.05. Hierarchical cluster analysis of DEGs was exhibited by heatmap, and KEGG annotation analysis and KEGG pathway enrichment analysis of DEGs were performed.

Real-Time Quantitative PCR Analysis (qRT-PCR)

The RNA of cardiac tissues was harvested and isolated using a Tri reagent, the concentration of which was quantified. The purified RNA was reversely transcribed into cDNA using the QuantiNova Reverse Transcription Kit and then amplified in a StepOnePlus PCR machine. The sequences for the primers are shown in Table 2.

Cell Cultivation

The H9c2 cell line was purchased from the Cell Resource Center, Shanghai Institutes for Biological Sciences, Chinese Academy of Sciences. The H9c2 cell line was cultivated in a DMEM medium supplemented with 10% FBS and 1%

Table 2 The Primer Sequences for the qRT-PCR Analysis

Primer	Sequence (Forward 5'-3')	Sequence (Reverse 5'-3')
Caspase-3	ATGGGAGCAAGTCAGTGGAC	CGTACCAGAGCGAGATGACA
Caspase-8	CCTAGACTGCAACCGAGAGG	GCAGGCTCAAGTCATCTTCC
Fas	ACCTCCAGTCGTGAAACCAT	CTCAGCTGTGTCTTGGATGC
Map3k5	GCCAGAGCTAAGTCCTGTGG	GCGCACTGTGATCTTCAAAA
Mapk9	CCCAAGGAATTGTTTGTGCT	CGAGTTCACGGTAGGCTCTC

penicillin-streptomycin. The cells were maintained in a humidified incubator with 5% CO_2 at 37 °C. During the logarithmic growth phase of the cells, trypsin-EDTA (0.25%) was used for trypsinization and subculture. Resuscitated third-generation cells were used for the experiments. DOX (0.5μM) was administered to induce the injury of cells. Simultaneously, KXD lyophilized powder (0, 50, 100, 200 μg/mL) was applied to the cells. All experiments in vitro were performed with a minimum of five independent experiments.

Tunel Staining

The cells were plated in a 6-well plate at the density of 3 ×10^5 cells per well and incubated with DMEM (10% FBS) in an incubator with an environment of 37°C and 5% CO_2. After 24 h, DMEM (10% FBS) containing different concentrations of KXD (0, 50, 100, 200 μg/mL) and DOX (0.5μM) were added in the wells respectively and incubated for 24 h, and DMEM (10% FBS) without KXD and DOX was as a vehicle. Apoptotic cells were tested using the one-step TUNEL apoptosis assay kit.

Western Blot

The H9c2 cells were plated in a 6-well plate at the density of 7 ×10^4 cells per well, and the subsequent cultivation referred to the procedure of TUNEL staining. The protein of heart tissues and H9c2 cells was harvested and lysed, the samples were fractionated by PAGE, transferred to PVDF membranes, blocked by a blocking buffer, and incubated with antibodies to Caspase-9, Fas, Bcl-2, Bax, Cx43, p-Cx43, ASK1, p-ASK1, JNK, p-JNK, and GAPDH at a dilution of 1:1000 overnight at 4°C. The membrane was washed three times with Tris-buffered saline with Tween 20 (TBST) for 10 min and incubated with HRP-linked anti-rabbit IgG or HRP-linked anti-mouse IgG for 1 h at room temperature. The strips were visualized using BeyoECL Plus. GAPDH was used as an internal control for normalization. All quantitative results of Western blot bands are summarized in Supplementary Materials (Tables S1–S17).

Statistical Analysis

Quantitative data are presented as mean ± standard deviation ($\bar{\chi} \pm s$) for normally distributed variables; otherwise, median and interquartile range (IQR) are reported. Quantitative data were assessed for normality using the Shapiro–Wilk test and for homogeneity of variance using Levene's test. Normally distributed data were analyzed by a one-way analysis of variance (ANOVA), followed by Tukey's post-hoc multiple comparison test for pairwise comparisons between groups. For non-normally distributed data, the Kruskal–Wallis test was applied, followed by Dunn's post-hoc test for pairwise comparisons. All analyses were performed using GraphPad Prism version 8.0. A value of $P<0.05$ was considered statistically significant.

Results

UPLC-Q-TOF-MS Analysis

UPLC-Q-TOF-MS was employed to explore the potential active ingredients of KXD. After oral administration of KXD, 11 compounds were identified in blood, including Protocatechuic acid-3-O-glucoside, Vanillic acid-4-O-β-D-glucoside, Neochlorogenic acid, Chlorogenic acid, 3,4,5-Trimethoxyphenyl 6-O-D-apio-β-D-furanosyl-β-D-glucopyranoside, Cryptochlorogenic acid, Caffeic acid, 3- Methoxy-L-tyrosine, Calycosin-7-O-glucoside, Azelaic acid, Ganoderic acid D. The results are shown in Figure 2A–C and Table 3.

KXD Significantly Improved Cardiac Function in cTnTR141W Transgenic Mice

Echocardiography of mice was performed after treatment for 4 weeks. As shown in Figure 3A and B, compared with the WT group, LVEDD, LVESD, LVDd, and LVDs of the $cTnT^{R141W}$ group were significantly increased ($P<0.0001$), and LVPW and LVAW were significantly thinner ($P<0.001$) with reduced EF and FS ($P<0.0001$). After treatment of KXD, LVEDD, LVESD, and LVD were reduced, and the LVPW and LVAW were significantly increased ($P<0.05$), along with increased EF and FS values ($P<0.0001$). After the treatment of captopril, LVEDD, LVESD, and LVD were reduced ($P<0.01$), the thickness of LVAWs was increased ($P<0.01$), and values of EF and FS were increased ($P<0.001$). These results indicated that KXD significantly inhibited the thinning of the ventricular wall and the enlargement of the left ventricle, and KXD improved cardiac function in $cTnT^{R141W}$ mice. As a positive control, captopril also improved cardiac function in $cTnT^{R141W}$ mice.

https://doi.org/10.2147/DDDT.S517404

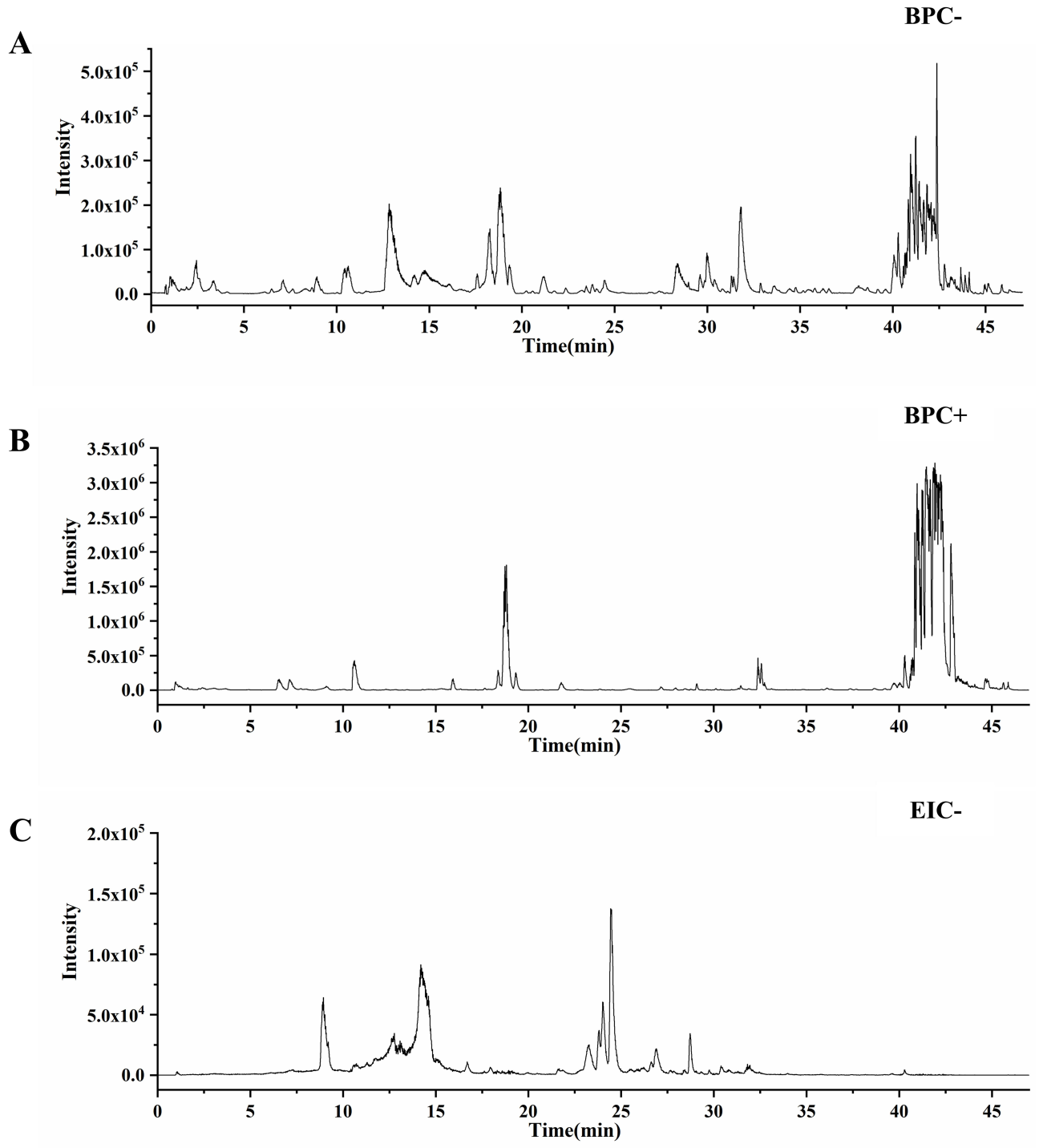

Figure 2 UPLC-Q-TOF-MS analysis of Kuoxin Decoction ingredients. (**A**) UPLC-HRMS base peak ion flow pattern (BPC) - negative ions of KXD plasma sample; (**B**) UPLC-HRMS base peak ion flow pattern (BPC) - positive ions of KXD plasma sample; (**C**) UPLC-HRMS extracted ion chromatogram (EIC) - negative ions of KXD plasma sample.

KXD Significantly Inhibited Cardiac Remodeling in cTnTR141W Transgenic Mice

As shown in Figure 4A and B, compared with the WT group, a large number of inflammatory cells were aggregated, the distribution of cardiomyocytes was in disorder, and the volume of cell nuclei was enlarged, accompanied by interstitial fibrosis in the heart of $cTnT^{R141W}$ transgenic mice ($P<0.0001$). Besides, the cross-sectional area of cardiomyocytes was increased in $cTnT^{R141W}$ transgenic mice compared with WT mice ($P<0.0001$). In addition, the inflammatory infiltrate

Table 3 Enriched Ingredients of Kuoxin Decoction in Plasma

No.	Identification	RT (min)	Adduct	*m/z*	ppm	CAS	Formula	Classification
1	Protocatechuic acid-3-O-glucoside	9.20	$[M-H]^-$	315.0722	1.3	7361-59-3	$C_{13}H_{16}O_9$	*Trichosanthes kirilowii* Maxim
2	Vanillic acid-4-O-β-D-glucoside	9.79	$[M-H]^-$	329.0878	0.3	32,142-31-7	$C_{14}H_{18}O_9$	*Trichosanthes kirilowii* Maxim, *Actinidia valvata* Dunn
3	Neochlorogenic acid	11.09	$[M-H]^-$	353.0878	−1.7	906-33-2	$C_{16}H_{18}O_9$	*Astragalus mongholicus* Bunge, *Salvia miltiorrhiza* Bunge, *Ilex pubescens* Hook. and Arn, *Neolitsea cassia* (L.) Kosterm, *Actinidia valvata* Dunn
4	Chlorogenic acid	13.19	$[M-H]^-$	353.0878	−1.1	327-97-9	$C_{16}H_{18}O_9$	*Astragalus mongholicus* Bunge, *Salvia miltiorrhiza* Bunge, *Ilex pubescens* Hook. and Arn, *Neolitsea cassia* (L.) Kosterm, *Actinidia valvata* Dunn
5	3,4,5-Trimethoxyphenyl 6-O-D-apio-β-D-furanosyl-β-D-glucopyranoside	13.72	$[M+FA-H]^-$	523.1668	−1.9	87,562-76-3	$C_{20}H_{30}O_{13}$	*Ilex pubescens* Hook. and Arn
6	Cryptochlorogenic acid	13.80	$[M-H]^-$	353.0878	−3.1	905-99-7	$C_{16}H_{18}O_9$	*Astragalus mongholicus* Bunge, *Ganoderma lucidum* (Leyss. Ex Fr.) Karst, *Salvia miltiorrhiza* Bunge, *Ilex pubescens* Hook. and Arn, *Neolitsea cassia* (L.) Kosterm, *Vitex negundo* L, *Actinidia valvata* Dunn
7	Caffeic acid	14.20	$[M-H]^-$	179.0350	2.8	331-39-5	$C_9H_8O_4$	*Astragalus mongholicus* Bunge, *Salvia miltiorrhiza* Bunge
8	3-Methoxy-L-tyrosine	14.40	$[M-H]^-$	210.0772	1.4	7636-26-2	$C_{10}H_{13}NO_4$	*Polygonatum kingianum* Collett & Hemsl
9	Calycosin-7-O-glucoside	19.89	$[M+FA-H]^-$	491.1195	−0.8	20,633-67-4	$C_{22}H_{22}O_{10}$	*Astragalus mongholicus* Bunge
10	Azelaic acid	23.22	$[M-H]^-$	187.0976	0.0	123-99-9	$C_9H_{16}O_4$	*Astragalus mongholicus* Bunge, *Polygonatum kingianum* Collett & Hemsl
11	Ganoderic acid D	33.98	$[M-H]^-$	513.2858	−1.4	108,340-60-9	$C_{30}H_{42}O_7$	*Ganoderma lucidum* (Leyss. Ex Fr.) Karst

was significantly reduced, the nucleus size was significantly reduced, the cells were neatly distributed, and the cross-sectional area of cardiomyocytes ($P<0.0001$) was decreased after the treatment with KXD. Meanwhile, captopril relieved the inflammatory infiltration and reduced the size of cardiomyocytes ($P<0.0001$). The size and weight of hearts in $cTnT^{R141W}$ transgenic mice were significantly increased compared with the WT group, and KXD and captopril decreased heart volume compared with the $cTnT^{R141W}$ group (Figure 4C).

KXD Significantly Inhibited Cardiomyocyte Apoptosis in cTnTR141W Transgenic Mice

RNA-seq was performed to determine the mechanism of KXD improving cardiac remodeling. KEGG pathway enrichment analysis of DEGs between the $cTnT^{R141W}$ group and the KXD group showed several pathways related to apoptosis, including Focal adhesion, cGMP-PKG signaling pathway, Hippo signaling pathway, and cAMP signaling pathway,[30–35] (Figure 5A), which indicated that KXD might regulate apoptosis (Figure 5A). Besides, KEGG enrichment analysis of Proteomic analysis indicated that the differentially expressed proteins between the KXD group and the $cTnT^{R141W}$ group were significantly enriched in the apoptosis pathway (Figure S1).

https://doi.org/10.2147/DDDT.S517404

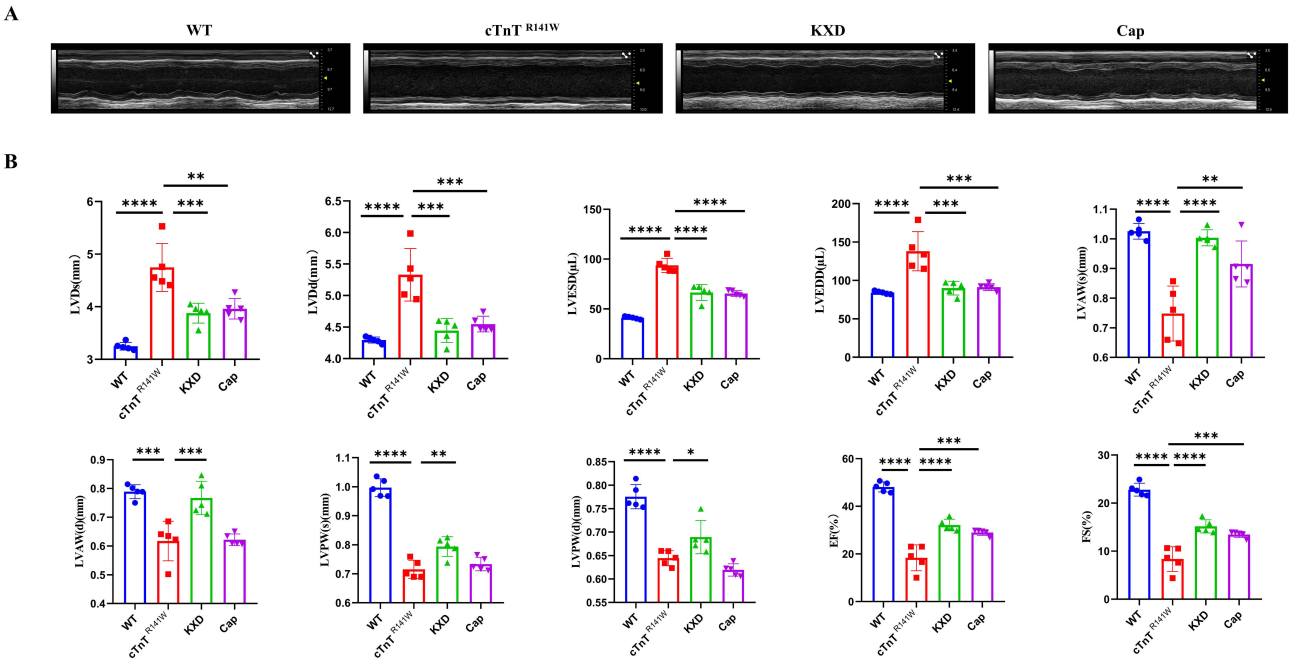

Figure 3 KXD significantly improved cardiac function in cTnT^{R141W} transgenic mice. (**A**). Echocardiography chart; (**B**). Quantitation of cardiac function. The data represent the mean ± SD from five independent experiments. *P<0.05 vs cTnT^{R141W} group, **P<0.01 vs cTnT^{R141W} group, ***P<0.001 vs cTnT^{R141W} group, ****P<0.0001 vs cTnT^{R141W} group. n=5.

The results of Figure 5B and C indicated numerous apoptotic cardiomyocytes in the heart tissue of cTnT^{R141W} transgenic mice compared with the WT group (P<0.0001), and KXD inhibited cardiomyocyte apoptosis (P<0.0001). The proportion of apoptotic cells decreased significantly after the treatment with captopril (P<0.0001). Caspase-3, Caspase-8, Caspase-9, Bcl-2, Bax, and Fas are the specific markers of apoptosis. Higher values of Bcl-2/Bax indicate greater anti-apoptotic ability. According to the results of Figure 5D, the mRNA expression level of *Caspase-3*(P<0.0001), *Caspase-8* (P<0.001) and *Fas* (P<0.01) was upregulated in cTnT^{R141W} transgenic mice, and *Caspase-3* (P<0.0001) and *Caspase-8* mRNA (P<0.05) were downregulated significantly by the treatment of KXD. As shown in Figure 5E and F, Caspase-9 protein was upregulated significantly (P<0.01) and Bcl-2/Bax was decreased (P<0.01) in cTnT^{R141W} transgenic mice.

KXD Significantly Alleviated Gap Junction Remodeling Between Cardiomyocytes in cTnTR141W Transgenic Mice

As shown in heatmap (Figure 6A), Pdgfb,[36] Adcy5, and Gnai1 are DEGs related to gap junctions, with upregulation of Pdgfb expression and downregulation of Adcy5 and Gnai1 expression in the KXD group. Cx43 is an important protein of GJs, and channel-dependent and -independent roles of Cx43 could overlap with the actin cytoskeletal-mediated regulation of barrier function.[37] As shown in Figure 6B, KXD participated in cellular community-eukaryotes, including focal adhesion, adherens junction, tight junction, and gap junction, they all belong to barrier-modulating cellular structures.[37] Besides, KEGG enrichment analysis of Proteomic analysis indicated that the differentially expressed proteins between the KXD group and the cTnT^{R141W} group were significantly enriched in gap junctions (Figure S1).These results indicated that KXD might regulate gap junctions through Cx43.

TEM was used to study the ultrastructure of GJs in greater detail. We used the width of the gap between two cardiomyocytes as an index to quantify the ultrastructural alterations of the gap junctions, with a wider gap indicating more serious damage to the superstructure of gap junctions.[28,29] As shown in Figure 6C, the width of the gap junction between cardiomyocytes in cTnT^{R141W} transgenic mice was increased compared with the WT group, which indicated that the structure of the GJs was impaired. After the treatment of KXD, the width of GJs was narrowed, and captopril also obviously shortened the width of GJs.

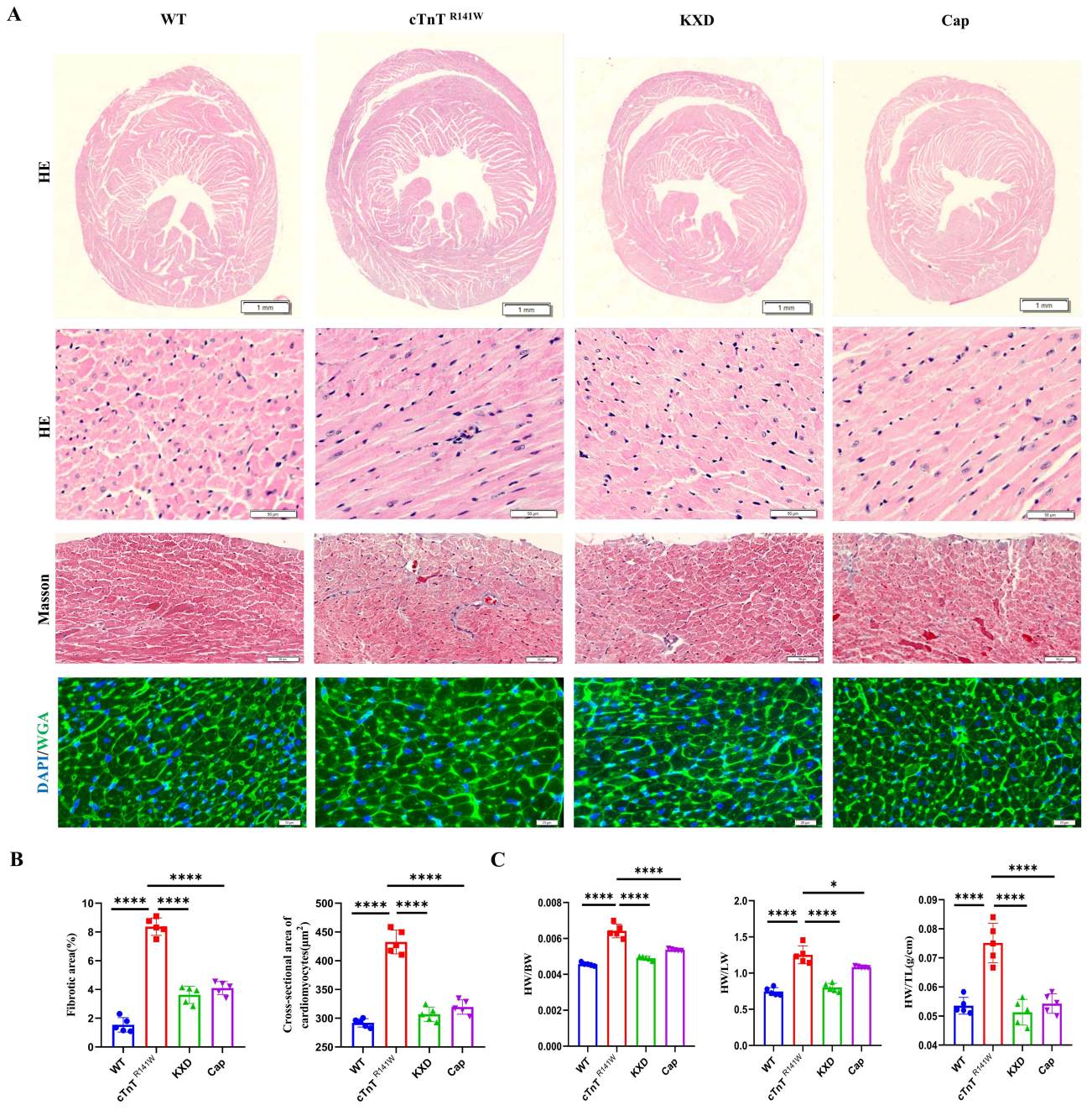

Figure 4 KXD significantly inhibited cardiac remodeling in cTnT^{R141W} transgenic mice. (**A**) H&E staining, Masson staining, and WGA staining; (**B**) Quantitation of fibrotic area and cross-sectional area of cardiomyocytes; (**C**) Quantitation of HW/BW, HW/LW, HW/TL. The data represent the mean ± SD from five independent experiments. *P<0.05 vs cTnT^{R141W} group, ****P<0.0001 vs cTnT^{R141W} group. n=5.

The results of immunofluorescent and Western blot indicated that the expression levels of Cx43 and p-Cx43 were downregulated in the heart of cTnT^{R141W} transgenic mice compared with the WT group (P<0.0001, P<0.001), and KXD could upregulated the distribution area (P<0.0001) and the expression levels of Cx43 protein (P<0.05) (Figure 6D–G). Captopril increased the distribution area (P<0.0001) and protein of Cx43 (P<0.05) (Figure 6D–G).

In cardiac tissue, GJs are formed primarily at the intercalated disk (ID), and ID is the site of contact between the ends of cardiomyocytes. WGA staining was used to label cardiomyocyte membranes, and the colocalization of WGA and Cx43 could reflect the distribution of Cx43 in cardiomyocytes. As shown in Figure 6H, Cx43 was commonly marked at ID in the WT group, but extensive Cx43 was also observed along cardiomyocyte lateral borders, representing impaired

https://doi.org/10.2147/DDDT.S517404

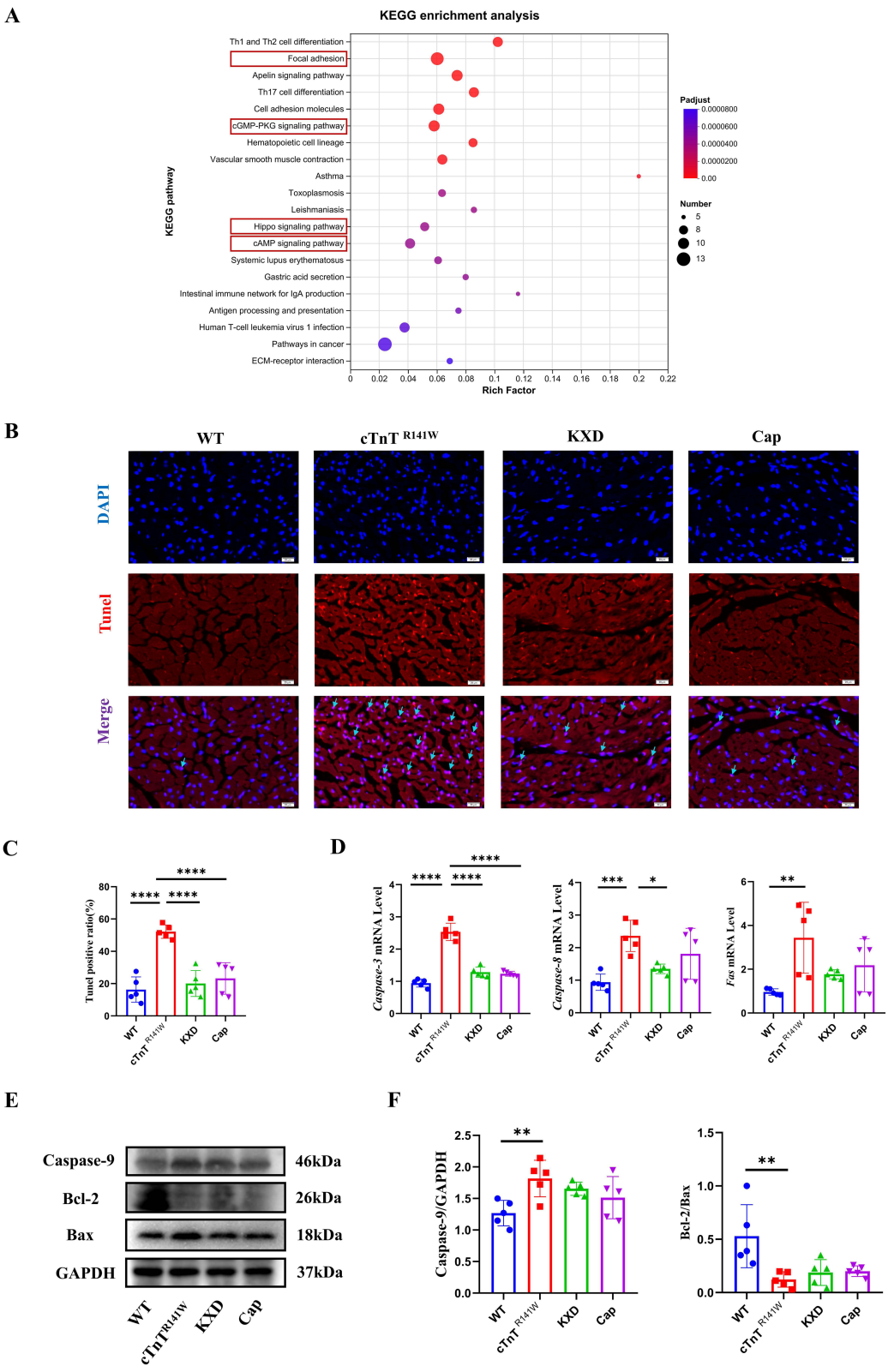

Figure 5 KXD significantly inhibited cardiomyocyte apoptosis in cTnT^{R141W} transgenic mice. (**A**) KEGG pathway enrichment analysis of DEGs between the cTnT^{R141W} group and the KXD group; (**B**) Tunel staining, the arrow indicates that apoptotic cardiomyocytes; (**C**) Quantitation of tunel positive ratio; (**D**) Quantitation of *Caspase-3, Caspase-8, Fas* mRNA, n=5; (**E**) The protein levels of Caspase-9, Bcl-2, and Bax were determined by Western blot in the heart; (**F**) Quantitation of Caspase-9, Bcl-2/Bax protein. The data represent the mean ± SD from five independent experiments. **P*<0.05 vs cTnT^{R141W} group, ***P*<0.01 vs cTnT^{R141W} group, ****P*<0.001 vs cTnT^{R141W} group, *****P*<0.0001 vs cTnT^{R141W} group. n=5.

 https://doi.org/10.2147/DDDT.S517404

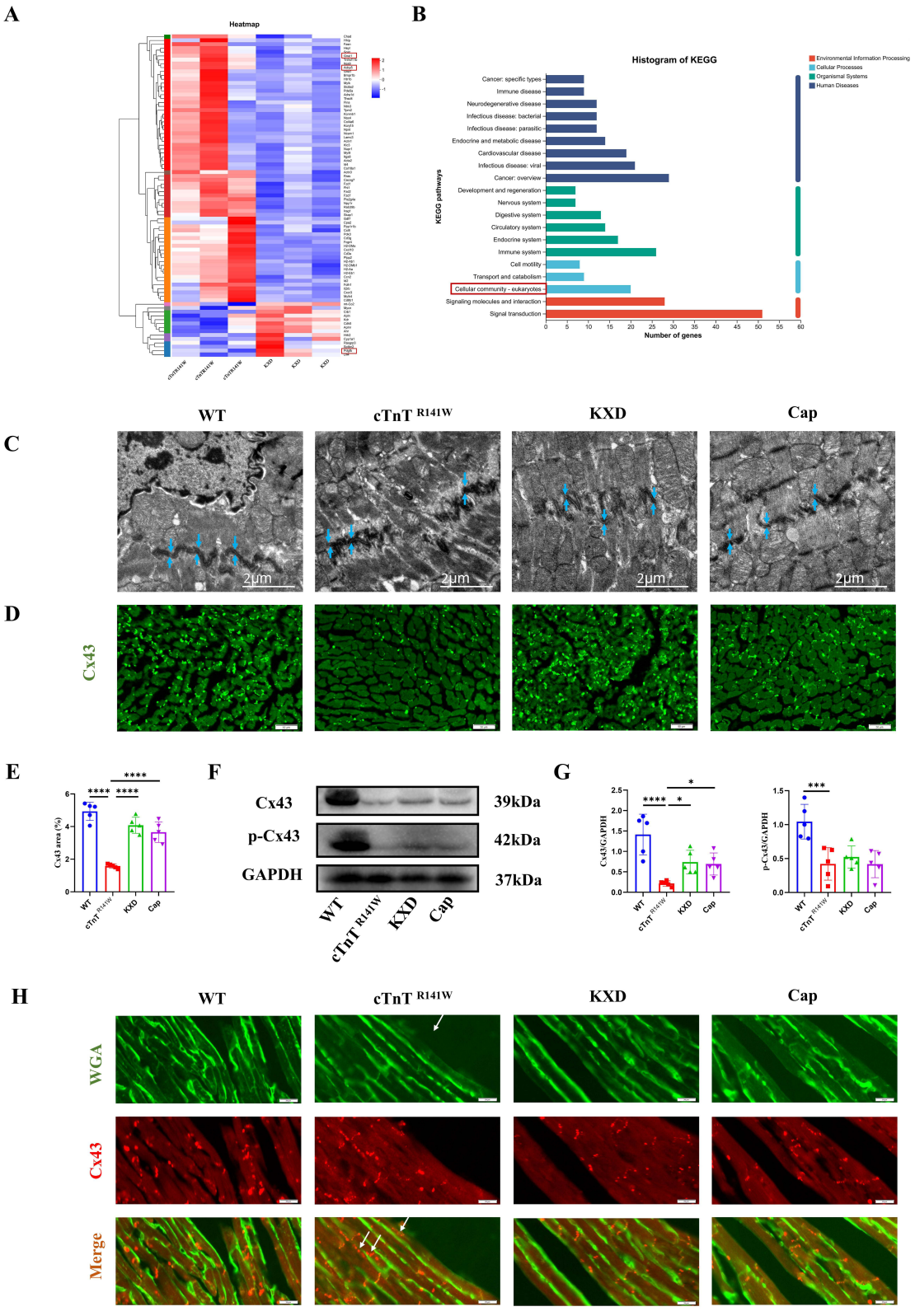

Figure 6 KXD significantly improved gap junction remodeling between cardiomyocytes in cTnT^{R141W} transgenic mice. (**A**) Heatmap of DEGs between the cTnT^{R141W} group and the KXD group; (**B**) KEGG annotations analysis of DEGs; (**C**) TEM imaged gap junctions, and the blue arrow indicates GJs, n=3; (**D**) Immunofluorescent localization of Cx43 (green) in cardiac myocardium; (**E**) Quantitation of the positive area of Cx43; (**F**). The protein levels of Cx43 and p-Cx43 were determined by Western blot in the heart; (**G**). Quantitation of Cx43, p-Cx43 proteins level; (**H**) Immunofluorescent localization of WGA (green) and Cx43 (red) in cardiac myocardium, and the white arrow indicates lateralized Cx43. The data represent the mean ± SD from five independent experiments. *P<0.05 vs cTnT^{R141W} group, ***P<0.001 vs cTnT^{R141W} group, ****P<0.0001 vs cTnT^{R141W} group. n=5.

https://doi.org/10.2147/DDDT.S517404

ultrastructure of GJs. Lateralized Cx43 was decreased in the KXD group and the captopril group. These results indicated that KXD and captopril significantly improved gap junction remodeling between cardiomyocytes in cTnT^{R141W} transgenic mice.

KXD Inhibited the Phosphorylation of ASK1 and JNK

The results of Figures 5 and 6 indicated that KXD could inhibit apoptosis and improve gap junction remodeling, and the ASK1/JNK signaling pathway is associated with regulating apoptosis. Besides, protein microarray results indicated that the expression of ASK1 and JNK proteins was increased in the model group, and KXD downregulated ASK1 and JNK proteins compared with the model group (Table S18). ASK1, JNK, and their phosphorylation were evaluated to explore whether KXD improved GJ remodeling and inhibited apoptosis by the ASK1/JNK signaling pathway. As shown in Figure 7A–C, the *Map3k5* (ASK1) and *Mapk9* (JNK) mRNA, ASK1, p-ASK1, and p-JNK proteins were upregulated in cTnT^{R141W} transgenic mice (P<0.05, P<0.001, P<0.05, P<0.01, P<0.01), and KXD significantly downregulated the expression level of *Mapk9* (JNK) mRNA (P<0.01). The results of Figure 7B and C indicated that KXD significantly decreased the expression levels of p-ASK1 (P<0.001) and p-JNK protein (P<0.05), and captopril had a similar effect, representing that KXD might inhibit apoptosis and alleviate gap junction remodeling by inhibiting the phosphorylation of ASK1 and JNK.

KXD Inhibits Apoptosis Induced by Doxorubicin in H9c2 Cells

As shown in Figure 8A, normal H9c2 cells were spindle-shaped, and multiple cells were clustered together. The cell morphology was changed under the intervention of DOX, and the nucleus volume became significantly larger and concave. Meanwhile, the proportion of apoptotic cells in the Model group was significantly increased compared with the control group (P<0.0001), and KXD (with dosages of 100μg/mL and 200μg/mL) downregulated the apoptosis rate (P<0.0001) (Figure 8B). After the intervention of DOX, the expression level of Caspase-9 protein was increased (P<0.05) with the trend of upregulated Fas protein, and the value of Bcl-2/Bax was significantly downregulated

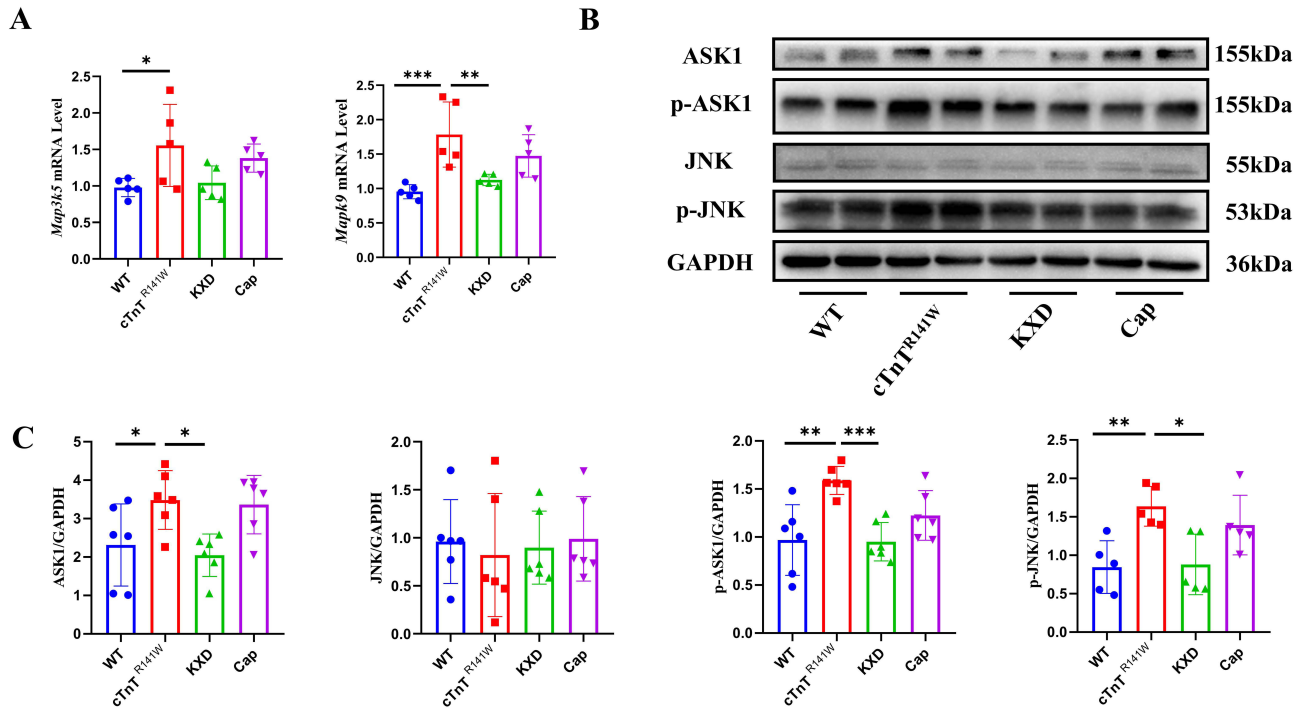

Figure 7 KXD inhibited the phosphorylation of ASK1 and JNK. (**A**). Quantitation of *Map3k5* (ASK1), *Mapk9* (JNK) mRNA in the heart, n=5; (**B**). The protein levels of ASK1, p-ASK1, JNK, and p-JNK were determined by Western blot in the heart; (**C**). Quantitation of ASK1, p-ASK1, JNK and p-JNK protein. The data represent the mean ± SD from five or six independent experiments. *P<0.05 vs cTnT^{R141W} group, **P<0.01 vs cTnT^{R141W} group, ***P<0.001 vs cTnT^{R141W} group. n=5 or 6.

 https://doi.org/10.2147/DDDT.S517404

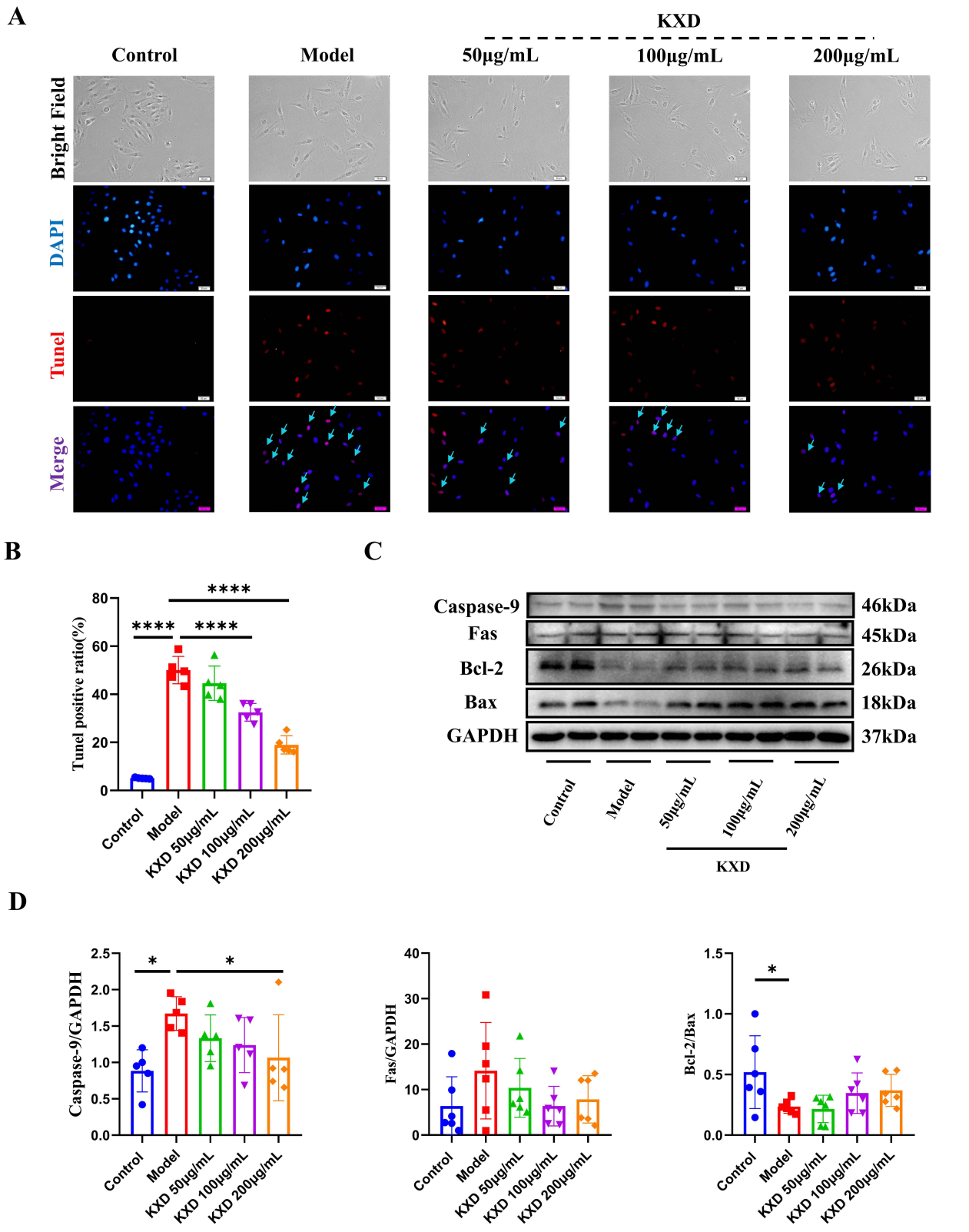

Figure 8 KXD inhibits apoptosis induced by doxorubicin in H9c2 cells. (**A**). Tunel staining, the arrow indicates apoptotic H9c2 cells; (**B**). Quantitation of positive ratio of apoptotic H9c2 cells; (**C**). The protein levels of Caspase-9, Fas, Bcl-2, and Bax were determined by Western blot; (**D**). Quantitation of Caspase-9, Fas, and Bcl-2/Bax protein. The data represent the mean ± SD from five or six independent experiments. **P*<0.05 vs the Model group, *****P*<0.0001 vs the Model group. n=5 or 6.

https://doi.org/10.2147/DDDT.S517404

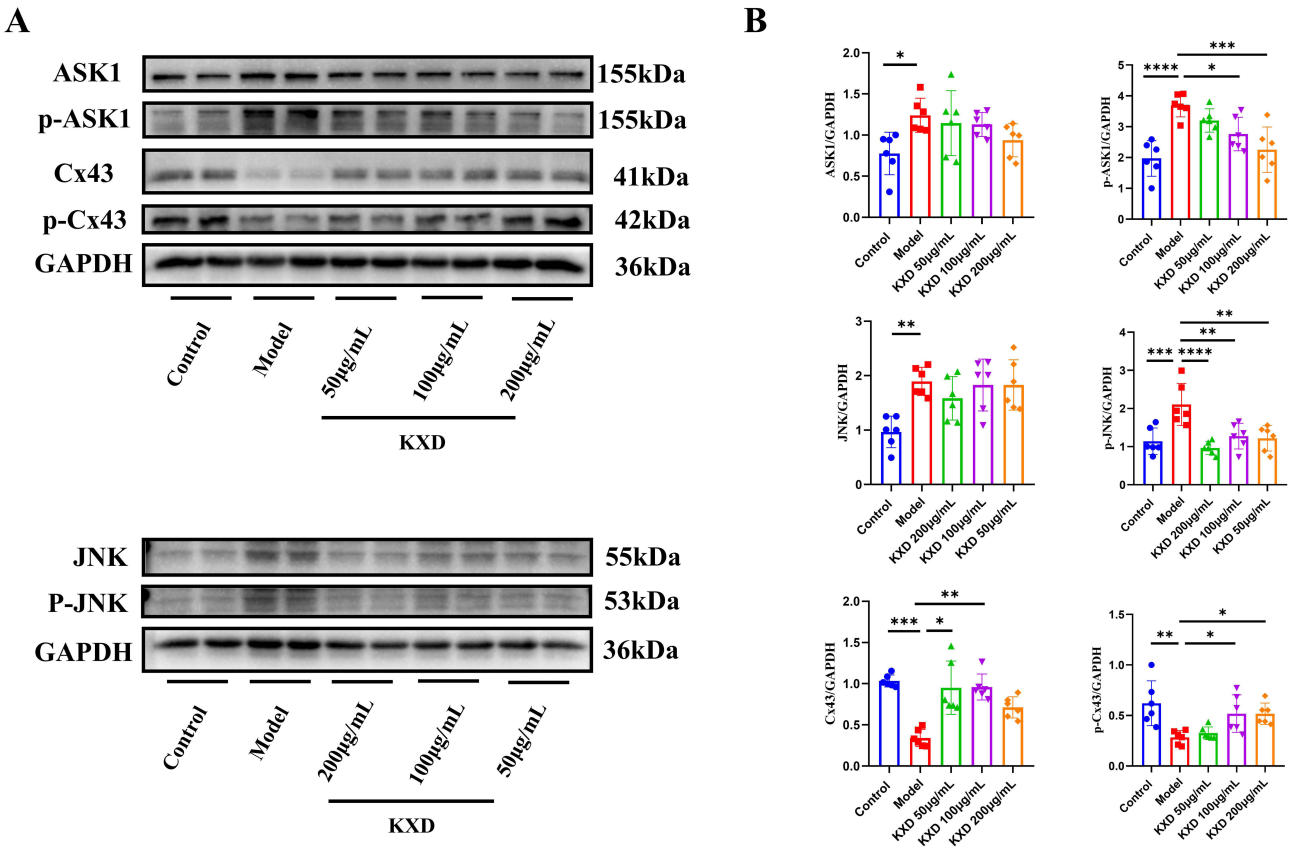

Figure 9 KXD inhibited the phosphorylation of ASK1 and JNK activated by doxorubicin in H9c2 cells. (**A**). The protein levels of ASK1, p-ASK1, Cx43, p-Cx43, JNK, and p-JNK were determined by Western blot in H9c2 cells; (**B**). Quantitation of ASK1, p-ASK1, JNK, p-JNK, Cx43, and p-Cx43 protein. The data represent the mean ± SD from six independent experiments. **P*<0.05 vs the Model group, ***P*<0.01 vs the Model group, ****P*<0.001 vs the Model group, *****P*<0.0001 vs the Model group. n=6.

(*P*<0.05) (Figure 8C and D). Although KXD did not downregulate Fas protein, Caspase-9 protein was significantly inhibited by KXD (200μg/mL) (*P*<0.05) (Figure 8C and D). These results are consistent with animal experiments, indicating that KXD inhibited apoptosis.

KXD Inhibited the ASK1/JNK/Cx43 Signaling Pathway in Doxorubicin-Induced H9c2 Cells

As shown in Figure 9A and B, the expression level of Cx43 and p-Cx43 protein was decreased with the intervention of DOX (*P*<0.001, *P*<0.01), and KXD significantly promoted the expression of Cx43 and p-Cx43 protein compared with the Model group (*P*<0.01, *P*<0.05). After the treatment of DOX, the expression levels of ASK1, p-ASK1, JNK, and p-JNK protein were upregulated in the Model group (*P*<0.05, *P*<0.0001, *P*<0.01, *P*<0.001), and KXD significantly inhibited the expression of p-ASK1, p-JNK protein (*P*<0.05, *P*<0.01) (Figure 9A and B). These results are consistent with those in animal tissues, indicating that KXD promoted the expression of Cx43, p-Cx43 and inhibited apoptosis induced by DOX by inhibiting the phosphorylation of the ASK1 and JNK.

Discussion

Dilated cardiomyopathy is a multifaceted myocardial disorder of unknown etiology, characterized by myocardial remodeling, progressive dilation, and impaired contractile function. Apoptosis, a significant contributing factor, results in cardiomyocyte loss, hypertrophy, fibrosis, and structural alterations, thereby aggravating ventricular remodeling and diminishing contractility.[38,39] Despite extensive investigation, the underlying mechanisms remain inadequately understood. Our previous clinical and preclinical studies have demonstrated that KXD enhances cardiac function and mitigates cardiac remodeling in DCM patients and animal models, potentially through the inhibition of apoptosis.[21–26,40,41] However, the upstream mechanisms underlying the protective effects of KXD against DCM have not been fully

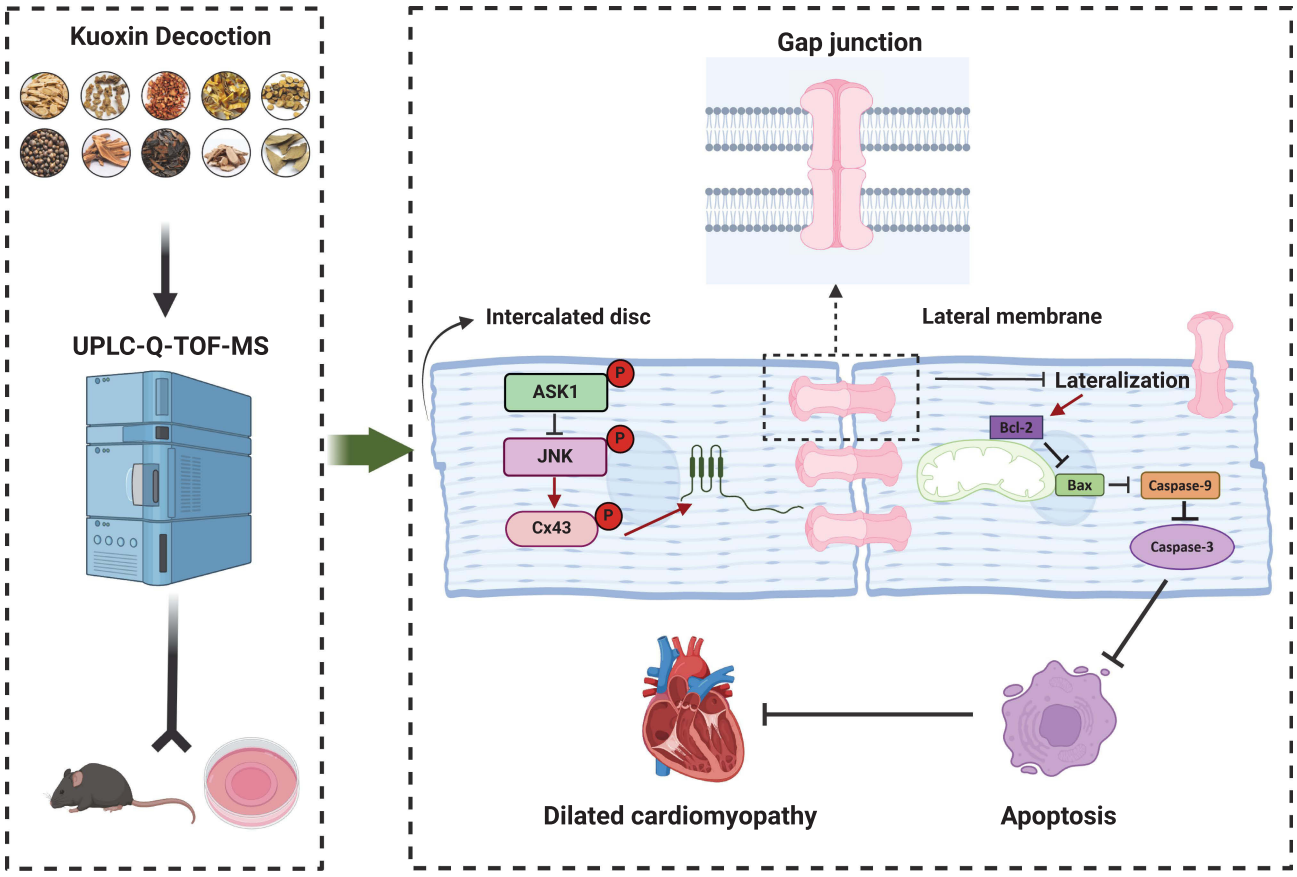

Figure 10 Mechanism diagram of the study. Kuoxin Decoction alleviated left ventricular remodeling by inhibiting cardiomyocyte apoptosis through ASK1/JNK/Cx43 signaling pathway. Red arrows indicate promotion and black inhibitors indicate inhibition. This presentation was created in BioRender. Ma, M. (2025) https://BioRender.com/b40k291.

delineated. This study demonstrated that KXD alleviates left ventricular remodeling in cTnT^{R141W} transgenic mice while attenuating cardiomyocyte apoptosis and gap junction remodeling, both in vivo and in vitro (Figure 10). Collectively, these findings provide an innovative strategy for developing more potent and safer therapeutics to alleviate DCM.

Genetic factors are a predominant cause of DCM, with 20~35% of cases exhibiting a familial history.[1] The R141W missense mutation in cTnT is a significant contributor to FDCM.[5] The cTnT^{R141W} mice manifest pathological phenotypes similar to DCM patients and are used in the study of DCM.[7,8] As shown in Figures 3 and 4, KXD effectively reduced left ventricular volume (P<0.001) and end-diastolic diameter (P<0.001), mitigated inflammatory cell infiltration and interstitial fibrosis (P<0.0001), and improved EF and FS (P<0.0001) in cTnT^{R141W} transgenic mice. Additionally, KXD inhibited cardiomyocyte apoptosis and down-regulated the expression of *Caspase-3* (P<0.0001), *Caspase-8* (P<0.05) mRNA in cTnT^{R141W} mice (Figure 5). These results indicate that KXD inhibits left ventricular remodeling and cardiomyocyte apoptosis in genetically induced DCM models, highlighting a clear novelty distinct from our previous studies.

The interaction between oncology and cardiology has gained increasing attention, particularly regarding the cardiotoxicity induced by anthracyclines like DOX, a widely used chemotherapeutic agent.[2,11] Our previous studies have shown that KXD significantly inhibited cardiomyocyte apoptosis in DOX-induced DCM models in both rats and mice. As shown in Figure 8, we found that KXD inhibits DOX-induced apoptosis (P<0.0001) and the expression of Caspase-9 protein (P<0.05) in H9c2 cells. Although the etiology of DCM remains largely unclear, genetic mutations and chemotherapy drugs are recognized as major contributing factors. Based on our previous research on DOX-induced animal models and the current study involving transgenic mice with genetic mutations, we have provided further evidence that KXD has a beneficial intervention effect on both genetically induced and chemotherapy-induced DCM, improving cardiomyocyte apoptosis in both models.

https://doi.org/10.2147/DDDT.S517404

Traditional Chinese Medicine has shown promising cardioprotective effects on cardiomyocytes, offering potential benefits in mitigating the side effects of Western treatments.[42,43] However, its complex composition and diverse therapeutic targets present significant challenges for pharmacological research.[44] Recent advances in bioinformatics have provided valuable insights into the mechanisms underlying cardiovascular diseases.[45–48] In this study, we used UPLC-Q-TOF-MS analysis and RNA sequencing to investigate the potential mechanisms by which KXD exerts its effects in treating DCM. As shown in Figure 2 and Table 3, we identified 11 compounds in KXD absorbed into the bloodstream through UPLC-Q-TOF-MS, including neochlorogenic acid, chlorogenic acid (CGA), cryptochlorogenic acid, caffeic acid, calycosin-7-O-glucoside, azelaic acid, and ganoderic acid D. Besides, UPLC-Q-TOF-MS was used to verify systemic absorption and ensure consistency across different biological models used, which is necessary to support the translational relevance of our experimental findings. Additionally, seven of these compounds play a role in regulating apoptosis and gap junctions, which help mitigate disease by reducing cell death.[49–55] Notably, CGA facilitates the binding of ASK1 and thioredoxin, resulting in decreased expression of JNK and p-JNK proteins.[56,57] Ca^{2+}-to-Src pathway modulates microglial gap junctions to induce glutamate release during hypoxia, and neochlorogenic acid and vitamin C inhibit InsP3-dependent Ca^{2+} signaling and prevent glutamate release under hypoxic conditions.[49] Similarly, caffeic acid phenethyl ester, the derivative of caffeic acid, alleviates hypoxia-induced downregulation of Cx43 and restores disrupted gap junction communication.[58,59] These findings suggest that KXD alleviates DCM by reducing apoptosis and modulating gap junction remodeling.

Gap junctions are membrane channel structures that facilitate intercellular communication, allowing the transfer of electrical and chemical signals. They are widely involved in processes such as cell injury, apoptosis, necrosis, and proliferation.[60] GJs are composed of connexins (Cx), with Cx43 being the most abundantly expressed connexin subtype in the human heart. The GJs formed by Cx43 mediate electrochemical coupling between cardiomyocytes, playing a crucial role in transmitting information and facilitating material exchange, which is essential for maintaining normal cardiac function.[61,62] In the study, RNA-seq was used to explore the molecular mechanisms underlying KXD's effects. KEGG annotation of DEGs in Figure 6B indicated that KXD participates in cellular community-eukaryotes, with Cx43 identified as a key protein interacting with the actin cytoskeleton to regulate barrier function. Decreased expression and altered subcellular distribution of Cx43 are associated with various structural cardiac diseases.[15,16,63] Moreover, numerous studies have identified Cx43 as a crucial target linked to cardiomyocyte apoptosis.[64–66] For instance, Wang's study reported apoptosis in corpus cavernosum cells of guinea pigs induced by Gap27, an inhibitor of gap junction.[67] Additionally, Cadmium exposure significantly inhibited gap junction intercellular communication, and downregulated Cx43, leading to increased apoptosis.[39] Besides, the degradation of Cx43 phosphorylation is closely associated with apoptotic processes.[17,18] Enhancing GJ function has been shown to inhibit apoptosis and improve left ventricular remodeling in dilated cardiomyopathy models.[13] In the study, KXD improved GJ integrity by narrowing the GJ width between cardiomyocytes in $cTnT^{R141W}$ transgenic mice (Figure 6C). KXD upregulated Cx43 ($P<0.05$) proteins and reduced the lateralization of Cx43 in $cTnT^{R141W}$ transgenic mice (Figure 6F–H), promoted Cx43 and phosphorylated Cx43 (p-Cx43) ($P<0.0.05$) proteins in H9c2 cells (Figure 9A and B). These findings suggest that KXD alleviates GJ remodeling, potentially inhibiting apoptosis and left ventricular remodeling (Figure 10).

The mitogen-activated protein kinase (MAPK) pathway is central to cardiomyocyte proliferation, differentiation, apoptosis, necrosis, and interstitial fibrosis.[68,69] ASK1, a MAPK kinase, activates JNK under oxidative stress, driving cellular damage and apoptosis.[70] ASK1 activation occurs when reduced thioredoxin oxidizes and dissociates from ASK1. Activated JNK inhibits Cx43 phosphorylation, disrupting gap junction internalization and intercellular communication, leading to gap junction remodeling and cardiomyocyte apoptosis.[71–73] Phosphorylated JNK has been shown to induce gap junction remodeling by affecting the internalization of gap junctions, potentially by inhibiting Cx43 phosphorylation through binding to its carboxyl terminus.[74] Furthermore, a JNK inhibitor reversed GJIC and Cx43 suppression.[75] As shown in Table S18, KXD reduced the expression levels of ASK1 and JNK in DOX-induced DCM rat models by protein microarray, which indicates that the therapeutic effects of KXD might be associated with the ASK1/JNK signaling pathway. In this study, we further explore the effect of KXD on genetic DCM ($cTnT^{R141W}$ transgenic mice) and chemotherapy-induced DCM (DOX-induced apoptosis in H9c2 cells). As shown in Figure 7A–C, KXD downregulated *Mapk9* (JNK) mRNA ($P<0.01$) and inhibited the expression of p-ASK1 ($P<0.001$) and p-JNK ($P<0.05$) proteins in

$cTnT^{R141W}$ transgenic mice. Similarly, KXD downregulated p-ASK1 ($P<0.05$) and p-JNK ($P<0.01$) proteins in vitro (Figure 9A and B). These findings support our hypothesis that KXD alleviates gap junction remodeling and cardiomyocyte apoptosis, which might be related to suppressing ASK1/JNK phosphorylation (Figure 10).

Limitation

While our study demonstrates that KXD upregulates Cx43 and inhibits p-ASK1/p-JNK, it's unclear whether Cx43 is the direct target of KXD. Due to limited funding and long experimental duration, the direct targeting effect of KXD on Cx43 has not been confirmed in the present study, and the lack of Co-IP antibodies for ASK1/JNK/Cx43 prevented direct validation of their molecular interactions. In future studies, we will construct $cTnT^{R141W}$ transgenic mice or H9c2 cells with Cx43 knockdown and ASK1/JNK overexpression, and intervene with KXD to further clarify whether ASK1/JNK/Cx43 is the direct target of KXD. Additionally, 7 compounds in KXD were identified that have the effect of regulating apoptosis or gap junction, we will explore the therapeutic effects of the active ingredient in KXD on DCM in the future.

Conclusion

In conclusion, our study demonstrates that KXD mitigates DCM by improving cardiac function, reducing ventricular remodeling, and inhibiting cardiomyocyte apoptosis in $cTnT^{R141W}$ transgenic mice and DOX-treated H9c2 cells. KXD appears to downregulate the ASK1/JNK signaling pathway, enhance Cx43 phosphorylation, and improve gap junction integrity, which may contribute to its anti-apoptotic and cardioprotective effects. While these findings provide preliminary mechanistic insights into KXD's potential in DCM therapy, further validation is needed to confirm its therapeutic applicability.

Abbreviations

ANOVA, a one-way analysis of variance; BW, body weight; Cap, captopril; CGA, chlorogenic acid; Cx43, connexin 43; DCM, dilated cardiomyopathy; DEGs, differentially expressed genes; DOX, doxorubicin; EF, ejection fraction; FS, fractional shortening; GJIC, gap junction intercellular communication; GJs, gap junctions; H&E, hematoxylin and eosin; HW, heart weight; ID, intercalated disk; KXD, Kuoxin Decoction; LV, left ventricular; LVAW, left ventricular anterior wall; LVDd, left ventricular end-diastolic diameter; LVDs, left ventricular end-systolic diameter; LVEDD, left ventricular end-diastolic dimension; LVESD, left ventricular end-systolic dimension; LVPW, left ventricular posterior wall; LW, lung weight; qRT-PCR, real-time quantitative PCR analysis; RNA-seq, RNA sequencing; SHUTCM, Shanghai University of Traditional Chinese Medicine; TCM, traditional Chinese medicine; TL, tibial length; WGA, wheat germ agglutinin; WT, wide-type.

Author Contributions

All authors made a significant contribution to the work reported, whether that is in the conception, study design, execution, acquisition of data, analysis and interpretation, or in all these areas; took part in drafting, revising or critically reviewing the article; gave final approval of the version to be published; have agreed on the journal to which the article has been submitted; and agree to be accountable for all aspects of the work.

Funding

This work was supported by the National Natural Science Foundation of China (grant numbers 81873264, 82004319, 82274463); the Science and Technology Plan Project of Shanghai Municipality (grant numbers 22Y11922000); and the Health Youth Talent Training Program of Shanghai Municipal Health Commission (grant numbers 2022YQ040).

Disclosure

The authors report no conflicts of interest in this work.

References

1. Weintraub RG, Semsarian C, Macdonald P. Dilated cardiomyopathy. *Lancet*. 2017;390(10092):400–414. doi:10.1016/s0140-6736(16)31713-5
2. Heymans S, Lakdawala NK, Tschöpe C, Klingel K. Dilated cardiomyopathy: causes, mechanisms, and current and future treatment approaches. *Lancet*. 2023;402(10406):998–1011. doi:10.1016/s0140-6736(23)01241-2
3. Yang J, Liao Y, Yuan J, et al. Chinese guideline on the diagnosis and treatment of dilated cardiomyopathy. *J Clin Cardiol*. 2018;34(05):421–434. doi:10.13201/j.issn.1001-1439.2018.05.001
4. Van Riet EE, Hoes AW, Wagenaar KP, Limburg A, Landman MA, Rutten FH. Epidemiology of heart failure: the prevalence of heart failure and ventricular dysfunction in older adults over time. A systematic review. *Eur J Heart Fail*. 2016;18(3):242–252. doi:10.1002/ejhf.483
5. Lu D, Shao HT, Ge WP, et al. Ginsenoside-Rb1 and tetramethylpyrazine phosphate act synergistically to prevent dilated cardiomyopathy in cTnTR141W transgenic mice. *J Cardiovasc Pharmacol*. 2012;59(5):426–433. doi:10.1097/FJC.0b013e318249509e
6. Juan F, Wei D, Xiongzhi Q, et al. The changes of the cardiac structure and function in cTnTR141W transgenic mice. *Int J Cardiol*. 2008;128 (1):83–90. doi:10.1016/j.ijcard.2008.03.006
7. Lu D, Wang J, Li J, et al. Meox1 accelerates myocardial hypertrophic decompensation through Gata4. *Cardiovasc Res*. 2018;114(2):300–311. doi:10.1093/cvr/cvx222
8. Lu D, Zhang L, Bao D, et al. Calponin1 inhibits dilated cardiomyopathy development in mice through the εPKC pathway. *Int J Cardiol*. 2014;173 (2):146–153. doi:10.1016/j.ijcard.2014.02.032
9. Chen NN, Ma XD, Miao Z, et al. Doxorubicin resistance in breast cancer is mediated via the activation of FABP5/PPARγ and CaMKII signaling pathway. *Front Pharmacol*. 2023;14:1150861. doi:10.3389/fphar.2023.1150861
10. Mozaffari S, Salehi D, Mahdipoor P, et al. Design and application of hybrid cyclic-linear peptide-doxorubicin conjugates as a strategy to overcome doxorubicin resistance and toxicity. *Eur J Med Chem*. 2021;226:113836. doi:10.1016/j.ejmech.2021.113836
11. Tomczyk MM, Cheung KG, Xiang B, et al. Mitochondrial Sirtuin-3 (SIRT3) prevents doxorubicin-induced dilated cardiomyopathy by modulating protein acetylation and oxidative stress. *Circ Heart Fail*. 2022;15(5):e008547. doi:10.1161/circheartfailure.121.008547
12. Shu G, Chen K, Li J, et al. Galangin alleviated Doxorubicin-induced cardiotoxicity by inhibiting ferroptosis through GSTP1/JNK pathway. *Phytomedicine*. 2024;134:155989. doi:10.1016/j.phymed.2024.155989
13. Yin H, Guo X, Chen Y, et al. TAB2 deficiency induces dilated cardiomyopathy by promoting RIPK1-dependent apoptosis and necroptosis. *J Clin Invest*. 2022;132(4):e152297. doi:10.1172/jci152297
14. Pang S, Dong W, Liu N, et al. Diallyl sulfide protects against dilated cardiomyopathy via inhibition of oxidative stress and apoptosis in mice. *Mol Med Rep*. 2021;24(6):852. doi:10.3892/mmr.2021.12492
15. Martins-Marques T, Catarino S, Gonçalves A, et al. EHD1 modulates Cx43 gap junction remodeling associated with cardiac diseases. *Circ Res*. 2020;126(10):e97–e113. doi:10.1161/circresaha.119.316502
16. Macquart C, Jüttner R, Morales Rodriguez B, et al. Microtubule cytoskeleton regulates Connexin 43 localization and cardiac conduction in cardiomyopathy caused by mutation in A-type lamins gene. *Hum Mol Genet*. 2019;28(24):4043–4052. doi:10.1093/hmg/ddy227
17. Kim IS, Ganesan P, Choi DK. Cx43 mediates resistance against MPP^+-induced apoptosis in SH-SY5Y neuroblastoma cells via modulating the mitochondrial apoptosis pathway. *Int J Mol Sci*. 2016;17(11):1819. doi:10.3390/ijms17111819
18. Yang Y, Yan X, Xue J, et al. Connexin43 dephosphorylation at serine 282 is associated with connexin43-mediated cardiomyocyte apoptosis. *Cell Death Differ*. 2019;26(7):1332–1345. doi:10.1038/s41418-019-0277-x
19. Qing C, Xinyi Z, Xuefei Y, Xindong X, Jianhua F. The specific connexin 43-inhibiting peptide Gap26 improved alveolar development of neonatal rats with hyperoxia exposure. *Front Pharmacol*. 2021;12:587267. doi:10.3389/fphar.2021.587267
20. Hao P, Jiang F, Cheng J, Ma L, Zhang Y, Zhao Y. Traditional Chinese medicine for cardiovascular disease: evidence and potential mechanisms. *J Am Coll Cardiol*. 2017;69(24):2952–2966. doi:10.1016/j.jacc.2017.04.041
21. Wang Y, Lin Y, Yuan S, et al. Clinical efficacy observation of Kuoxin recipe in the treatment of dilated cardiomyopathy. *Shanghai J Traditional Chin Med*. 2017;51(06):60–62. doi:10.16305/j.1007-1334.2017.06.018
22. Wu Q, Peng L, Dong Y, et al. Clinical observations of Kuoxin recipe for dilated cardiomyopathy of both Qi and Yin deficiency combined with blood stasis patient. *J Emergency Traditional Chin Med*. 2021;30(11):1940–1943+1946. doi:10.3969/j.issn.1004-745X.2021.11.014
23. Wu Q, Yang A, Zhou D, Wang Y. Left ventricular reverse remodeling in dilated cardiomyopathy. *Adv Cardiovasc Dis*. 2019;40(06):885–889. doi:10.16806/j.cnki.issn.1004-3934.2019.06.012
24. Fan H, Yang A, Wang Y, et al. effect of kuoxinfang on sarcoplasmic reticulum Ca2+-ATPase and phosphoprotein in rats with dilated cardiomyopathy. *Modern Trad Chin Med Materia Medica-World Sci Technol*. 2018;20(02):233–238. doi:10.11842/wst.2018.02.015
25. Wu Q, Dong Y, Wang Y, et al. Improvement effect of kuoxin recipe on myocardial fibrosis in rats with dilated cardiomyopathy through TGF-β1/Smad2 pathway. *Modern Trad Chin Med Materia Medica-World Sci Technol*. 2022;24(01):243–251. doi:10.11842/wst.20210822009
26. Peng L, Ma M, Dong Y, et al. Kuoxin Decoction promotes lymphangiogenesis in zebrafish and in vitro based on network analysis. *Front Pharmacol*. 2022;13:915161. doi:10.3389/fphar.2022.915161
27. Zhou W, Zhu Z, Xiao X, et al. Jiangzhi Granule attenuates non-alcoholic steatohepatitis by suppressing TNF/NFκB signaling pathway-a study based on network pharmacology. *Biomed Pharmacother*. 2021;143:112181. doi:10.1016/j.biopha.2021.112181
28. Sun JD, Liu Y, Yuan YH, Li J, Chen NH. Gap junction dysfunction in the prefrontal cortex induces depressive-like behaviors in rats. *Neuropsychopharmacology*. 2012;37(5):1305–1320. doi:10.1038/npp.2011.319
29. Dong R, Han Y, Jiang L, et al. Connexin 43 gap junction-mediated astrocytic network reconstruction attenuates isoflurane-induced cognitive dysfunction in mice. *J Neuroinflammation*. 2022;19(1):64. doi:10.1186/s12974-022-02424-y
30. Ye L, Liu R, Lin P, Wang W. Krüppel-like transcription factor 16 transcriptional up-regulation of cellular retinoic acid-binding proteins-2 promotes the invasion and migration and inhibits apoptosis of retinoblastoma cells by regulating integrin-β1/focal adhesion kinase /extracellular signal-regulated kinase pathway. *Bioengineered*. 2022;13(2):3694–3706. doi:10.1080/21655979.2021.2024977
31. Chen CI, Chen YC, Chang CY, Huang BM, Chen YC. Clerodane diterpene induces apoptosis/anoikis and suppresses migration and invasion of human bladder cancer cells through the histone deacetylases, integrin-focal adhesion kinase, and matrix metalloproteinase 9 signalling pathways. *Hum Exp Toxicol*. 2022;41:9603271221143040. doi:10.1177/09603271221143040

32. Huang Q, Ma J, Wu H, Zhou J, Jiang L, Fei X. PDE-5-inhibited BMSCs alleviate high glucose-induced myocardial fibrosis and cardiomyocyte apoptosis by activating the cGMP/PKG pathway. *Front Biosci*. 2023;28(7):155. doi:10.31083/j.fbl2807155
33. Akintunde JK, Akintola TE, Aliu FH, Fajoye MO, Adimchi SO. Naringin regulates erectile dysfunction by abolition of apoptosis and inflammation through NOS/cGMP/PKG signalling pathway on exposure to Bisphenol-A in hypertensive rat model. *Reprod Toxicol*. 2020;95:123–136. doi:10.1016/j.reprotox.2020.05.007
34. She G, Du JC, Wu W, et al. Hippo pathway activation mediates chemotherapy-induced anti-cancer effect and cardiomyopathy through causing mitochondrial damage and dysfunction. *Theranostics*. 2023;13(2):560–577. doi:10.7150/thno.79227
35. Yang WJ, Han FH, Gu YP, et al. TGR5 agonist inhibits intestinal epithelial cell apoptosis via cAMP/PKA/c-FLIP/JNK signaling pathway and ameliorates dextran sulfate sodium-induced ulcerative colitis. *Acta Pharmacol Sin*. 2023;44(8):1649–1664. doi:10.1038/s41401-023-01081-y
36. Zhao F, Yan J, Zhao J, et al. Effect of platelet-derived growth factor-BB on gap junction and connexin43 in rat penile corpus cavernosum smooth muscle cells. *Andrologia*. 2019;51(3):e13200. doi:10.1111/and.13200
37. Strauss RE, Gourdie RG. Cx43 and the actin cytoskeleton: novel roles and implications for cell-cell junction-based barrier function regulation. *Biomolecules*. 2020;10(12):1656. doi:10.3390/biom10121656
38. Del Re DP, Amgalan D, Linkermann A, Liu Q, Kitsis RN. Fundamental mechanisms of regulated cell death and implications for heart disease. *Physiol Rev*. 2019;99(4):1765–1817. doi:10.1152/physrev.00022.2018
39. Zou H, Zhuo L, Han T, et al. Autophagy and gap junctional intercellular communication inhibition are involved in cadmium-induced apoptosis in rat liver cells. *Biochem Biophys Res Commun*. 2015;459(4):713–719. doi:10.1016/j.bbrc.2015.03.027
40. Zhao H, Liu L, Fei F, et al. Study on cardioprotective effect of Kuoxinfang on tnnt2a mutant zebrafish. *Shanghai J Traditional Chin Med*. 2019;53 (02):72–76. doi:10.16305/j.1007-1334.2019.02.019
41. Dong Y, Ma M, Peng L, et al. Study on myocardial lymphangiogenesis disorder in dilated cardiomyopathy mice induced by doxorubicin and the protective mechanism of kuoxin decoction. *Modern Trad Chin Med Materia Medica-World Sci Technol*. 2023;25(10):3293–3303. doi:10.11842/wst.20230905001
42. Quickfall D, Jakubovic B, Zipursky JS. Angiotensin-converting-enzyme inhibitor-induced angioedema. *Cmaj*. 2021;193(20):E735. doi:10.1503/cmaj.202308
43. Wang M, Wang M, Zhao J, Xu H, Xi Y, Yang H. Dengzhan Shengmai capsule attenuates cardiac fibrosis in post-myocardial infarction rats by regulating LTBP2 and TGF-β1/Smad3 pathway. *Phytomedicine*. 2023;116:154849. doi:10.1016/j.phymed.2023.154849
44. Shi S, Mao X, Lv J, et al. Qi-Po-Sheng-Mai granule ameliorates Ach-CaCl(2) -induced atrial fibrillation by regulating calcium homeostasis in cardiomyocytes. *Phytomedicine*. 2023;119:155017. doi:10.1016/j.phymed.2023.155017
45. Liu X, Peng S, Tang G, et al. Fasting-mimicking diet synergizes with ferroptosis against quiescent, chemotherapy-resistant cells. *EBioMedicine*. 2023;90:104496. doi:10.1016/j.ebiom.2023.104496
46. Petersen TB, de Bakker M, Asselbergs FW, et al. HFrEF subphenotypes based on 4210 repeatedly measured circulating proteins are driven by different biological mechanisms. *EBioMedicine*. 2023;93:104655. doi:10.1016/j.ebiom.2023.104655
47. Huang Y, Zhang K, Jiang M, et al. Regulation of energy metabolism by combination therapy attenuates cardiac metabolic remodeling in heart failure. *Int J Biol Sci*. 2020;16(16):3133–3148. doi:10.7150/ijbs.49520
48. Zhao C, Li S, Zhang J, et al. Current state and future perspective of cardiovascular medicines derived from natural products. *Pharmacol Ther*. 2020;216:107698. doi:10.1016/j.pharmthera.2020.107698
49. Socodato R, Portugal CC, Rodrigues A, et al. Redox tuning of Ca (2+) signaling in microglia drives glutamate release during hypoxia. *Free Radic Biol Med*. 2018;118:137–149. doi:10.1016/j.freeradbiomed.2018.02.036
50. Komeili-Movahhed T, Heidari F, Moslehi A. Chlorogenic acid alleviated testicular inflammation and apoptosis in tunicamycin induced endoplasmic reticulum stress. *Physiol Int*. 2023;110(1):19–33. doi:10.1556/2060.2023.00132
51. Fan Y, Yang Y, Li Y, et al. Chlorogenic acid promotes angiogenesis and attenuates apoptosis following cerebral ischaemia-reperfusion injury by regulating the PI3K-Akt signalling. *Pharm Biol*. 2022;60(1):1646–1655. doi:10.1080/13880209.2022.2110599
52. Bai X, Liu Y, Cao Y, Ma Z, Chen Y, Guo S. Exploring the potential of cryptochlorogenic acid as a dietary adjuvant for multi-target combined lung cancer treatment. *Phytomedicine*. 2024;132:155907. doi:10.1016/j.phymed.2024.155907
53. Pan Y, Liu D, Wei Y, et al. Azelaic Acid exerts antileukemic activity in acute myeloid leukemia. *Front Pharmacol*. 2017;8:359. doi:10.3389/fphar.2017.00359
54. Zhang D, Liu Y, Luo Z, et al. The novel thioredoxin reductase inhibitor A-Z2 triggers intrinsic apoptosis and shows efficacy in the treatment of acute myeloid leukemia. *Free Radic Biol Med*. 2020;146:275–286. doi:10.1016/j.freeradbiomed.2019.11.013
55. Yuan H, Xu Y, Luo Y, Zhang JR, Zhu XX, Xiao JH. Ganoderic acid D prevents oxidative stress-induced senescence by targeting 14-3-3ε to activate CaM/CaMKII/NRF2 signaling pathway in mesenchymal stem cells. *Aging Cell*. 2022;21(9):e13686. doi:10.1111/acel.13686
56. Gao W, Wang C, Yu L, et al. Chlorogenic acid attenuates dextran sodium sulfate-induced ulcerative colitis in mice through MAPK/ERK/JNK pathway. *Biomed Res Int*. 2019;2019:6769789. doi:10.1155/2019/6769789
57. Kang JB, Son HK, Park DJ, Jin YB, Shah FA, Koh PO. Modulation of thioredoxin by chlorogenic acid in an ischemic stroke model and glutamate-exposed neurons. *Neurosci Lett*. 2024;825:137701. doi:10.1016/j.neulet.2024.137701
58. Lee KW, Chun KS, Lee JS, Kang KS, Surh YJ, Lee HJ. Inhibition of cyclooxygenase-2 expression and restoration of gap junction intercellular communication in H-ras-transformed rat liver epithelial cells by caffeic acid phenethyl ester. *Ann N Y Acad Sci*. 2004;1030:501–507. doi:10.1196/annals.1329.062
59. Chen CC, Kuo CY, Chen RF. Role of CAPE on cardiomyocyte protection via connexin 43 regulation under hypoxia. *Int J Med Sci*. 2016;13 (10):754–758. doi:10.7150/ijms.15847
60. Dhein S, Salameh A. Remodeling of cardiac gap junctional cell-cell coupling. *Cells*. 2021;10(9):2422. doi:10.3390/cells10092422
61. Zhu Y. Gap junction-dependent and -independent functions of connexin43 in biology. *Biology*. 2022;11(2):283.doi:10.3390/biology11020283. doi:10.3390/biology11020283
62. Rodríguez-Sinovas A, Sánchez JA, Valls-Lacalle L, Consegal M, Ferreira-González I. Connexins in the heart: regulation, function and involvement in cardiac disease. *Int J Mol Sci*. 2021;22(9):4413. doi:10.3390/ijms22094413
63. Hesketh GG, Shah MH, Halperin VL, et al. Ultrastructure and regulation of lateralized connexin43 in the failing heart. *Circ Res*. 2010;106 (6):1153–1163. doi:10.1161/circresaha.108.182147

64. Ge Z, Diao H, Yu M, et al. Connexin 43 mediates changes in protein phosphorylation in HK-2 cells during chronic cadmium exposure. *Environ Toxicol Pharmacol*. 2017;53:184–190. doi:10.1016/j.etap.2017.06.003
65. Chen K, Chen L, Ouyang Y, et al. Pirfenidone attenuates homocysteine-induced apoptosis by regulating the connexin 43 pathway in H9C2 cells. *Int J Mol Med*. 2020;45(4):1081–1090. doi:10.3892/ijmm.2020.4497
66. Kim D, Mouritzen U, Larsen BD, Roy S. Inhibition of Cx43 gap junction uncoupling prevents high glucose-induced apoptosis and reduces excess cell monolayer permeability in retinal vascular endothelial cells. *Exp Eye Res*. 2018;173:85–90. doi:10.1016/j.exer.2018.05.003
67. Wang Y, Wang J, Hao Z, et al. Inhibition of gap junction communication between cells can induce apoptosis of corpus cavernosum smooth muscle in Guinea pigs. *Andrologia*. 2022;54(1):e14287. doi:10.1111/and.14287
68. Yue J, López JM. Understanding MAPK signaling pathways in apoptosis. *Int J Mol Sci*. 2020;21(7):2346. doi:10.3390/ijms21072346
69. Li R, Guo Y, Zhang Y, Zhang X, Zhu L, Yan T. Salidroside ameliorates renal interstitial fibrosis by inhibiting the TLR4/NF-κB and MAPK signaling pathways. *Int J Mol Sci*. 2019;20(5):1103. doi:10.3390/ijms20051103
70. Lai J, Li A, Yue L, Zhong H, Xu S, Liu X. Participation of ASK-1 in the cardiomyocyte-protective role of mechanical ventilation in a rat model of myocardial infarction. *Exp Biol Med*. 2023;248(18):1579–1587. doi:10.1177/15353702231191205
71. Li H, Yang Q, Huang Z, et al. Dual-specificity phosphatase 12 attenuates oxidative stress injury and apoptosis in diabetic cardiomyopathy via the ASK1-JNK/p38 signaling pathway. *Free Radic Biol Med*. 2022;192:13–24. doi:10.1016/j.freeradbiomed.2022.09.004
72. Chen X, Ma W, Yao Y, et al. Serum deprivation-response protein induces apoptosis in hepatocellular carcinoma through ASK1-JNK/p38 MAPK pathways. *Cell Death Dis*. 2021;12(5):425. doi:10.1038/s41419-021-03711-x
73. Liang J, Chen P, Li C, et al. IL-22 down-regulates Cx43 expression and decreases gap junctional intercellular communication by activating the JNK pathway in psoriasis. *J Invest Dermatol*. 2019;139(2):400–411. doi:10.1016/j.jid.2018.07.032
74. Zhang FF, Morioka N, Nakashima-Hisaoka K, Nakata Y. Spinal astrocytes stimulated by tumor necrosis factor-α and/or interferon-γ attenuate connexin 43-gap junction via c-jun terminal kinase activity. *J Neurosci Res*. 2013;91(6):745–756. doi:10.1002/jnr.23213
75. Changchien CY, Sung MH, Chang HH, Tsai WC, Peng YS, Chen Y. Uremic toxin indoxyl sulfate suppresses myocardial Cx43 assembly and expression via JNK activation. *Chem Biol Interact*. 2020;319:108979. doi:10.1016/j.cbi.2020.108979